UiT
THE ARCTIC UNIVERSITY OF NORWAY

Faculty of Biosciences, Fisheries and Economics
Department of Arctic and Marine Ecology

Spectral analysis and image classification of the dwarf shrub *Empetrum nigrum* (L.) by means of remote sensing data.

—

Edurne Ibarrola Ulzurrun
Master thesis in Biology BIO-3950 - 15th May 2014

Supervisors:
Associate Professor Kari Anne Bråthen, UiT The Arctic University of Norway
Associate Professor Lennart Nilsen, UiT The Arctic University of Norway

Co-supervisor:
Professor Michael E. Shaepman, University of Zürich (CH)

UNIVERSITY OF TROMSØ

TABLE OF CONTENTS

SUMMARY

Empetrum nigrum dominates in alpine and northern part of Norway. It is an allelopathic species that can reduce both productivity and biodiversity in ecosystems. The study focuses on identifying and determining different cover of *E. nigrum* by means of remote sensing data within two regions of Northern Norway, Ifjord in Finnmark and Troms areas. Field data were collected within 50 study points and *E. nigrum* was cover recorded. Field data were compared with Landsat 7 ETM+ and Landsat 8 OLI satellite images. Remote sensing is a practical and cost-effective tool to classify land cover and study vegetation changes when large areas are measured. Landsat images were chosen due to good cover, spatial resolution, free availability and its long history, which allows going back in time.

Besides, small field plots were measured in the Troms area with ASD FieldSpec spectroradiometer in order to extract a spectral signature of *E. nigrum*, in coexistence with other common species. Several supervised and unsupervised classification algorithms were performed on the satellite data using the ENVI image processing software. It resulted that neither the specific features (evergreen appearance with a dense cover of tiny leaves with glands producing the allelopathic compound Batatasin-III, and its dominance over vast land areas) nor the ASD FieldSpec measurements of *E. nigrum*, were suitable for extracting a spectral signature of the species that made a good classification. However, the best result was obtained using a spectral unmixing classification applied to radiometric corrected images in both areas separately. A spectral library created by endmember determination from Landsat data was used for this classification. An evaluation (Pearson correlation), was made in both areas combined as well as in Ifjord study area and Tromsø study area separately. No-

correlation between the ground truth data and the data extracted from the spectral unmixing analysis was observed when both areas where combined (r = 0.15). Whereas, a positive correlation appeared when analysing both areas separately (Tromsø, r = 0.55 and Ifjord r = 0.57). Landsat has several issues concerning to endmember determination, spatial, temporal and spectral resolution, as well as data acquisition problem. However, some solutions are proposed. So, it is concluded that Landsat is a good option for *E. nigrum* retrieval. The opinion is that future studies need to include these improvements or solutions, in order to achieve an *E. nigrum* classification with a higher correlation coefficient from Landsat imagery.

KEY WORDS: remote sensing, Landsat, *Empetrum nigrum*, Northern Norway, spectral unmixing classification, ASD FieldSpec, ENVI.

INTRODUCTION

Assessing and monitoring the state of the earth surface is a key requirement for global change research. Global climate change has pronounced effects in ecosystems and arctic and alpine regions dominated by dwarf shrubs (Walker et al., 2005). These ecosystems have been more affected due to a faster warming effect than in other areas (Wookey et al., 2009). Elmendorf et al., 2012 studied that global warming has positive effects on canopy height and abundance of shrubs in arctic and alpine tundra ecosystems (Elmendorf et al., 2012). Additionally, allelopathic species can affect whole ecosystems in ways that reduce both ecosystems productivity (Bråthen et al., 2010) and biodiversity (Pellissier et al., 2010). This increment of shrub abundance due to global warming, as well as *E. nigrum* being an allelophatic species, makes this plant an important species in arctic and alpine areas. Besides, it is both very dominant (Keech et al., 2005) in heath vegetation and very common in tundra in general (Tybirk et al., 2000, Bråthen et al., 2010). According to Xie et al. 2008 about the importance of vegetation mapping, *E. nigrum* mapping could be an essential tool for assessing natural and land-use changes in arctic and alpine environments through quantifying vegetation cover from local to broader scales, i.e. alpine tundra, at a given time point to over continuous period.

E. nigrum has a circumboreal distribution in acidic and nutrient poor soils (Tybirk et al., 2000, Keech et al., 2005, Nilsson et al., 1998). It dominates in alpine and northern part of Norway (Pellissier et al., 2010, Nilsson et al., 1998) and its dominance is related to clonal and dense pattern of growth (Pellissier et al., 2010, Tybirk et al., 2000), phenolic production to sequester nutrients and Batatasin-III (allelophatic compound) production (Bråthen et al., 2010, Nilsson et al., 1998, Keech et al., 2005, Gallet et al., 1999, Wallstedt et al., 2005, Mallik, 2008, Wallstedt et al., 2000, Wallstedt et al., 1997,

Nilsson et al., 2000). Thus *E. nigrum* inhibits productivity of these environments (Bråthen et al., 2010).

Remote sensing offers a practical and cost-effective means to classify land cover or study vegetation changes, especially when large areas are measured (Xie et al., 2008, Reinke and Jones, 2006). It involves the measurement of the electromagnetic radiation (reflected sunlight) from features on the Earth's surface (Smith, 2006, Aplin, 2004, Goodchild, 1994), providing a basic representation of land cover variation on the surface. The satellite sensor captures data about an object's spectral signature (Smith, 2006, Xie et al., 2008) and it can be identified from the imagery according to its unique spectral features. Vegetation has specific reflectance curves (Smith, 2006) dictated by various plant attributes (Figure 1 (Smith, 2006)). It is possible to distinguish vegetation classes at various levels in the hierarchy interpreting specific features of the vegetation species such as image colour, texture, tone, pattern, etc. (Xie et al., 2008) rather than taxonomic or floristic criteria (Franklin and Wulder, 2002). *E. nigrum* has several features that indicate it is likely to have a unique way of reflecting radiation wavelengths recorded by satellite sensor devices, i.e. unique spectral signature. The first feature of *E. nigrum* is somewhat special because of glands developing on its leaves in which a compound called Batatasin-III is produced (Nilsson et al., 1998, Gallet et al., 1999, Wallstedt et al., 2005). The second one, *E. nigrum* is an evergreen species with a dense cover of tiny leaves (Tybirk et al., 2000, Lid and Lid, 2007), which is not shared by many species. Finally, the third feature refers to its dominance over vast land areas (Pellissier et al., 2010, Nilsson et al., 1998).

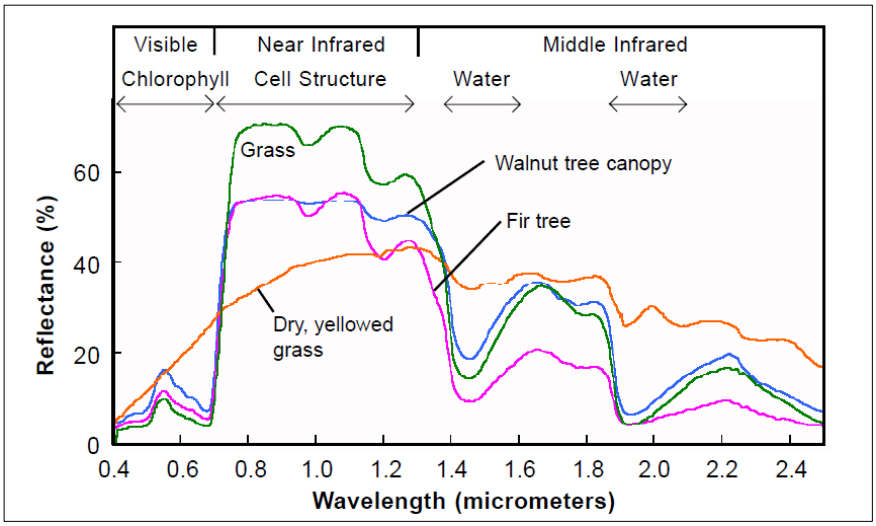

Figure 1. "Reflectance spectra of different types of green vegetation compared to a spectral curve for senescent (dry, yellowed) leaves. Different portions of the spectral curves for green vegetation are shaped by different plant components, as show at the top" (Smith, 2006).

Landsat might have the longest history and widest use in monitoring and land cover mapping of the Earth from the space since the first Landsat satellite was launched in 1972. A series of more sophisticated multispectral imaging sensors, named TM (Thematic Mapper), have been added, ranging from Landsat 4 to 7 (Enhanced Thematic Mapper Plus, ETM+) and being Landsat 8 OLI , the last launched in 2013 (Xie et al., 2008). Landsat provides medium to coarse spatial resolution images, i.e. 30 meters in multispectral bands (Aplin, 2005, Kerr and Ostrovsky, 2003, Xie et al., 2008). It is often used to map vegetation at community level and not at species level even though some dominant species can be possibly discriminated (Xie et al., 2008).

Comparative analyses of old and new satellite images could potentially be a source of information about where and to what extent the cover of *E. nigrum* has actually changed. Therefore, it is needed to assess how well and at what accuracy *E. nigrum* can

be classified and cover estimated from remote sensing images. In the case of Landsat, its long history can be used for performing time-serial analyses. Hence, it was chosen for carrying out this study.

Image classification is the process of extracting differentiated endmembers or spectral classes (Xie et al., 2008) (e.g. vegetation species such as *E. nigrum* or a forest of *Betula pubescens*). Many classification algorithms are available such as supervised classification (Spectral Unmixing and Maximum Likelihood) and unsupervised classification (K-Means and Isodata), neural net classification and spectral angle mapper (Keshava and Mustard, 2002, Van Der Meer and De Jong, 1999, Smith, 2006). However, there is no ideal vegetation classification approach and there are no pixels assigned to a single endmember but a proportion of multiple endmembers or classes (Franklin and Wulder, 2002, Aplin, 2004, Van Der Meer and De Jong, 1999). These make both vegetation classification and extraction a hard and difficult task, reducing the accuracy of classification due to the spectral confusion they create.

The study aim is to evaluate the possibility of mapping different cover degree of *Empetrum nigrum* by means of remote sensing data.

Within two regions of Northern Norway, E. *nigrum* cover was recorded inside 50 study points. These points were applied as ground truth data and then compared to Landsat ETM+ 7 and Landsat OLI 8 images covering these two regions.

The dominant role of *E. nigrum* in many northern and high latitude habitats, and its ability to prevent other plant species establishment, is partly attributed to leaf glands production of the allelophathic compound, Batatasin-III. Hyperspectral studies with ASD FieldSpec were applied to test whether Batatasin-III gives a spectral signature that

can be traced in plant leaves, and if successful, whether the coverage of *E. nigrum* can be observed based on the spectral library of Batatasin-III. Furthermore small scale ground truth data were compared to ASD FieldSpec hyperspectral data.

In order to accomplish the study aim some questions have to be answered. Firstly, can a spectral signature of *E. nigrum* be extracted from the Landsat channel data as well as by ASD FieldSpec spectroradiometer measurements in the laboratory, which could support and improve the *E. nigrum* cover classification?

Secondly, can an accurate spectral library be created with different predefined classes (endmembers) and thus help to achieve a good classification result?

The main questions are: a) is Landsat remote sensing data suitable for mapping *E. nigrum* cover classes? and b) what is the best classification method for mapping different cover of *E. nigrum*? In order to answer the two main questions correlations between field measurements of *E. nigrum* and the different Landsat classification results were performed.

MATERIAL AND METHODS

Following Hall (1991), the method consisted of five steps (Hall et al., 1991) (1) obtaining remote sensing images of a scene, (2) using field observations to determine the coverage of ground plots, (3) determining the geographic coordinates in the image pixels and locating the pixels corresponding to the ground plots, (4) atmospherically adjustment of images, (5) computing the spectral characteristics. For a better understanding a flow diagram was created (Figure 2).

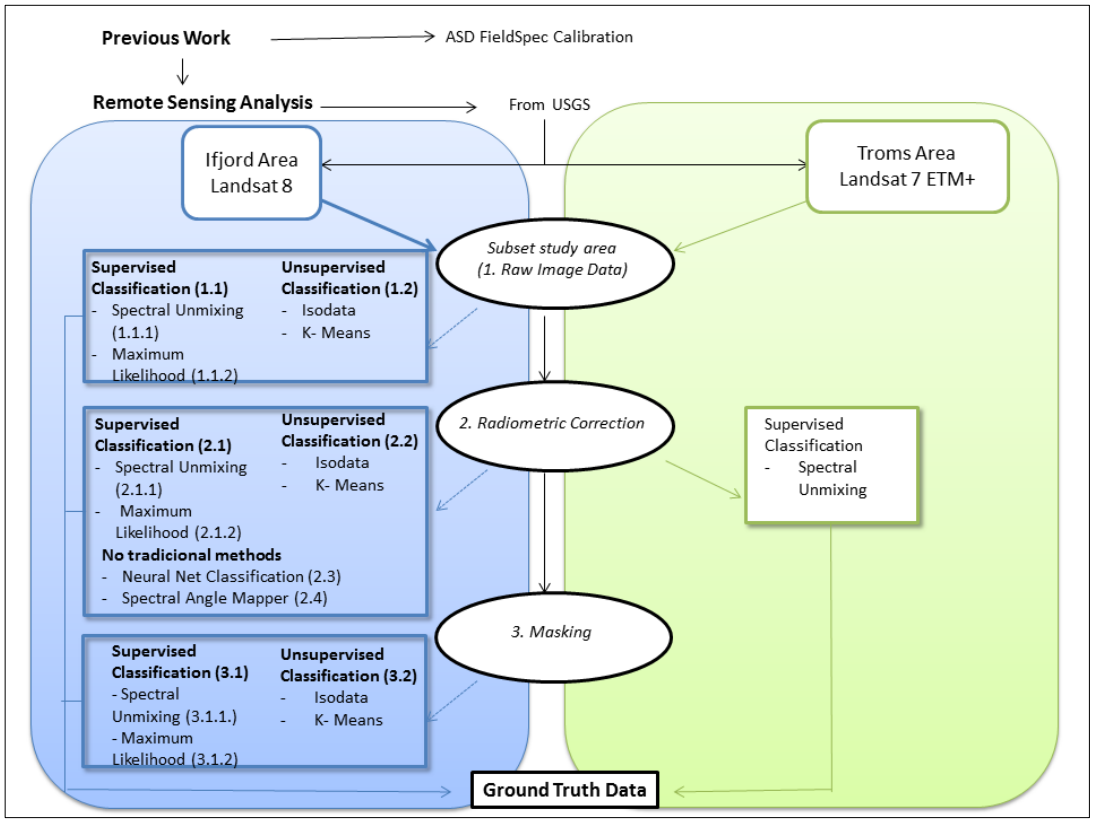

Figure 2. Flow Diagram of every method followed in the study. Scenes from Ifjord and Tromsø from U.S. Geological Survey (USGS). In bold, main steps carried out in the study. Lighter squares, Landsat scenes of each area. Circle, steps and corrections of the images. Squares, method performed in each step and in each area, representing as two columns. Left (in blue): classification methods performed in Ifjord scene. Right (in green): classification methods performed in Tromsø scene. Number in each methods refers to each section in Ifjord area analyses (Process and Results).

ASD FieldSpec Analyses

Batatasin-III calibration with ASD FieldSpec

In previous spectral analyses, ASD FieldSpec spectroradiomenter was used for measuring the spectrum of Batatasin-III in pure form. On top of a green leaf three depressions of absorption are shown (Figure 3), 1675 nm, 2150 nm and 2270 nm of Batatasin-III (test kindly conducted by Zbynek Malenovsky, University of Zurich). In addition, Batatasin-III of *E. nigrum* leaves were calibrated with spectroradiometer (ASD FieldSpec) using a chromatography (HPLC) technique. Pearson correlation was made in order to analyse if Batatasin-III content *E. nigrum* leaves extracted from HPLC technique were correlated with the predicted values of Batatasin-III determined by ASD FieldSpec means (APPENDIX I).

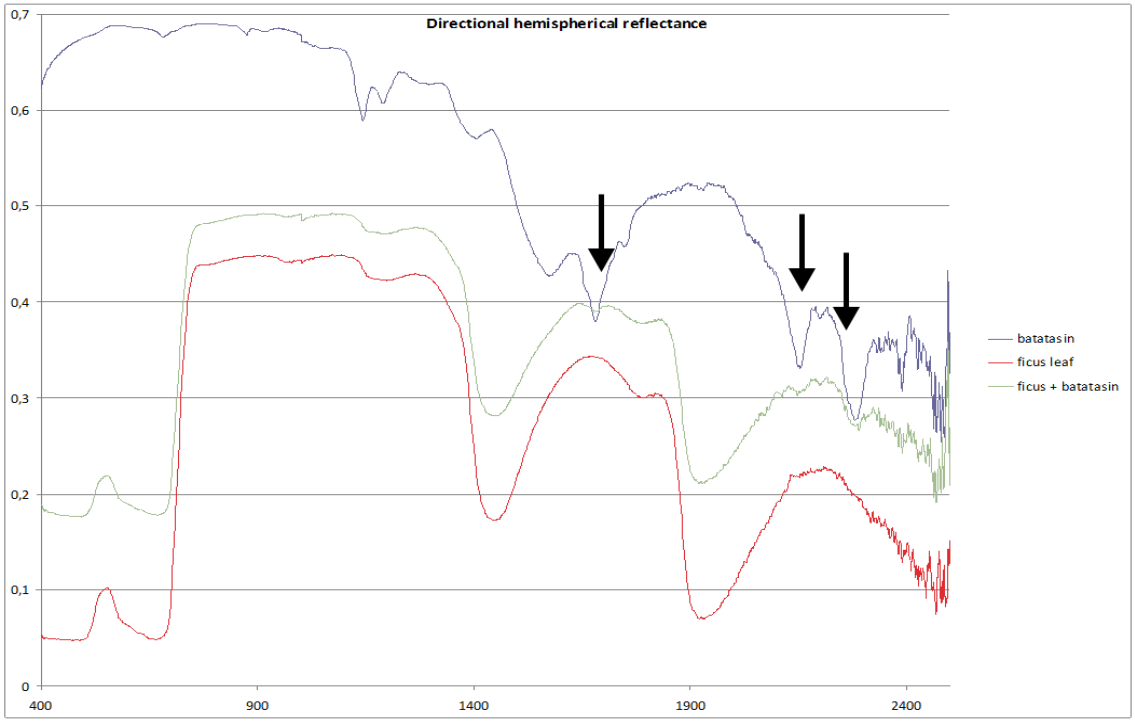

Figure 3. Batatasin-III (blue), Ficus spp. (red) and Ficus spp. + Batatasin-III (green) spectra (Malenovsky, 2012).

Batatasin-III validation with ASD FieldSpec

ASD Fieldspec spectroradiometer was used to retrieve measurements from small circular field plots (approximately 0.05 m^2) in the beginning of July 2013. The measurements were carried out in three different areas of Troms County, Tromsøya, Rebbenesøya and Lyfjorden (Figure 4), in order to extract a specific signature of *E. nigrum* in field in coexistence with other common species of the habitat. Therefore, a spectral library is created for the later spectral analysis. In total 58 spectra were retrieved from plots with varying *E. nigrum* cover. Within each plot, 3 separate ASD Fieldspec spectra were taken at different locations in the plot and then, averaged. Within each plot *E. nigrum* was registered in coexistence with other common species, such as *Vaccinum myrtillus, Vaccinum uligonosum, Vaccinum vitis-idea, Arctostaphyllus alpina, Rubus chamaemorus, Cornus suecica,* as well as graminoids, lichens, and bryophytes. Moreover, some leaves of *E. nigrum* were collected and dried during 24 hours at 35˚C. Then, they were measured in the laboratory with ASD FieldSpec in order to get a pure spectral signature of *E. nigrum* for using afterwards as a part of a spectral library.

Besides, validation of Batatasin-III content in leaves was made. The calibration performed with the HPLC technique was used in order to know whether Batatasin-III content was dependent on *E. nigrum* coverage or not. ASD FieldSpec delivered the validation for each spectrum and its predictable value for the Batatasin-III content (APPENDIX II). The average of Batatasin-III predicted value for each point was then correlated with the ASD FieldSpec field measurements of *E. nigrum* in Tromsøya, Rebbenesøya and Lyfjorden, in order to study a correlation between coverage of *E. nigrum* and levels of Batatasin-III.

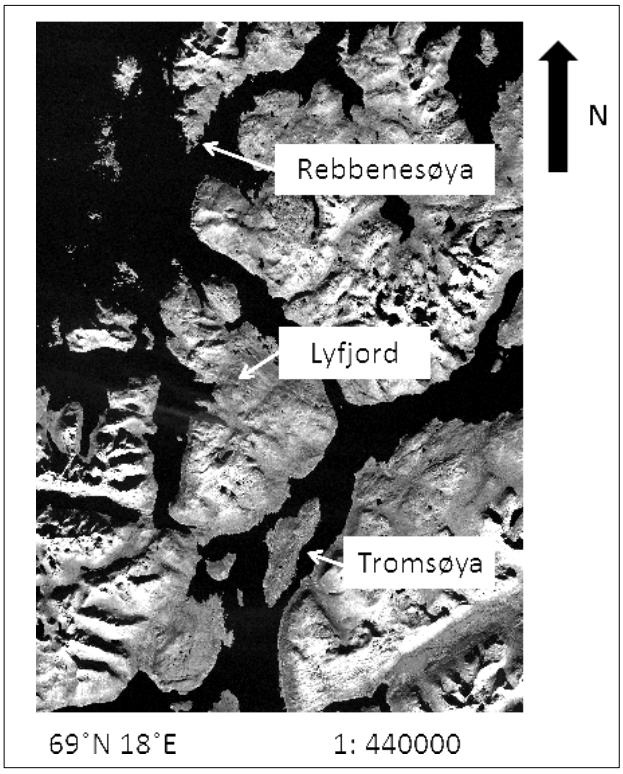

Figure 4. Map from Troms County pointing the areas of the ASD FieldSpec measurements. Tromsø, Rebbenesøya and Lyfjord.

Study Area

Two sites located within the northern boreal region of Norway were selected for this study, i.e. Tromsø, Troms County (69º N, 18Eº) and Ifjord, Finmark (71º N, 27º E) (Figure 5). Finmark and Troms County in Norway form the northern boundary of the European continent, delineated by the Barents Sea in the north and by birch forests and continuous taiga in the south (Pellissier et al., 2010, Bråthen et al., 2007, Bråthen et al., 2010). The fennoscandic mountain area is classified as erect low-shrub tundra, belonging to the sub-arctic mountain tundra. The landscape is heath dominated, with mainly *E. nigrum* (Bråthen et al., 2007, Pellissier et al., 2010, Keech et al., 2005,

Shevtsova et al., 2005) by *Betula nana*, *Vaccinum spp.*, graminoids such as *Avenella flexuosa*, *Deschampsia spp.*, *Carex spp.*, and dichotyleons (*Cornus spp.*).

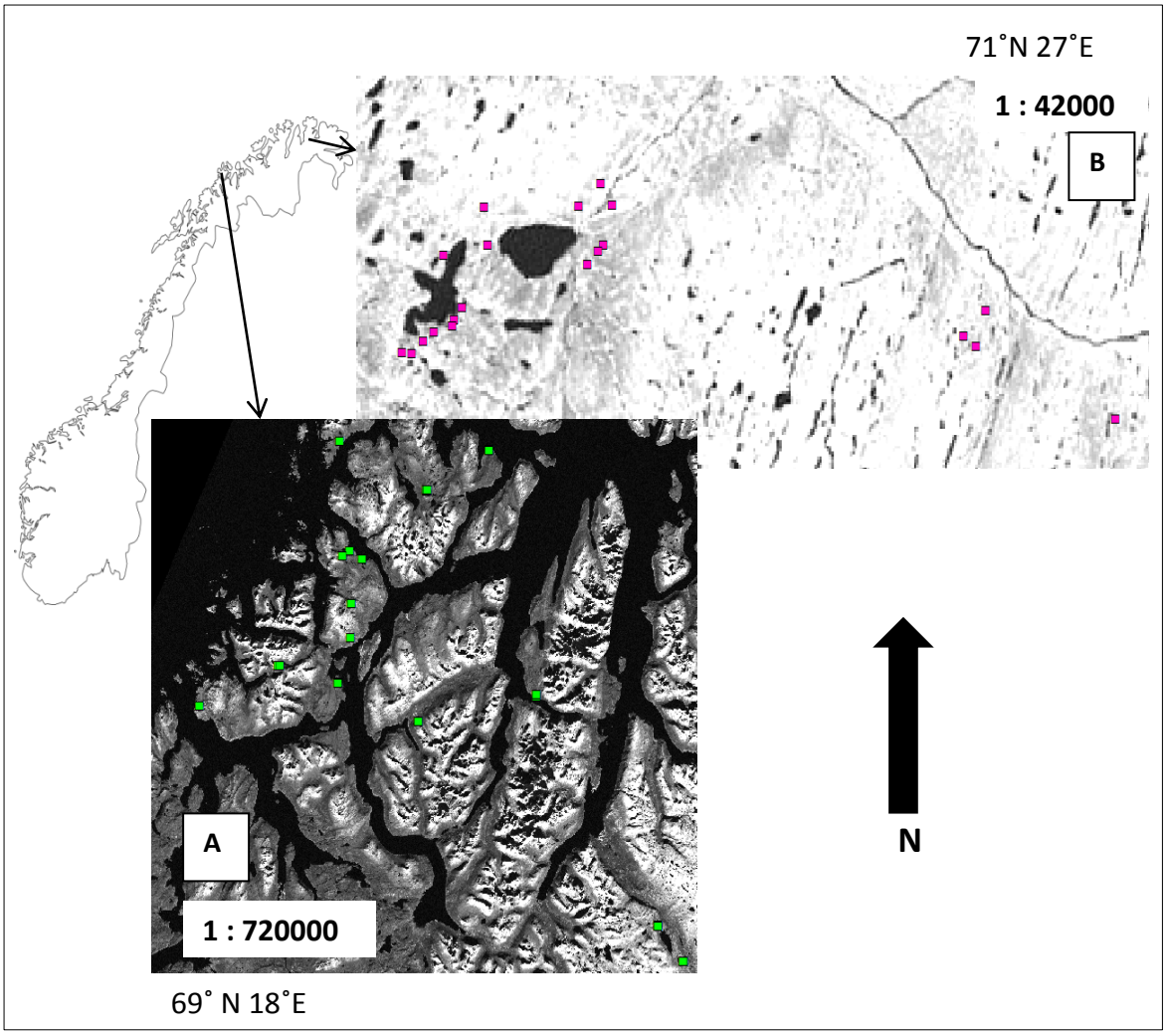

Figure 5. General map from Norway pointing the study areas in Tromsø (A), green squares; and Ifjord (B), pink squares.

Collection of research material

Remote sensing data

Landsat 8 OLI and Landsat 7 ETM+ scenes were downloaded from U.S Geological survey (USGS) http://earthexplorer.usgs.gov/ (U.S Geological Survey, 2014, Hall et al.,

1991). Landsat 8 OLI scene both path:row are 194:10 from Ifjord area. The scene was acquired on the 17th of August of 2013. Landsat 8 OLI has 8 multispectral bands, 2 thermal bands and one panchromatic band. Landsat 7 ETM+ scene is 197:11 (path:row) from Tromsø area. It was acquired on the 9th of September of 1999 and it has 6 multispectral bands, 1 thermal band and 1 panchromatic band (Table 1).

Table 1. Comparison of bands wavelengths between Landsat 7 ETM+ and Landsat 8 OLI.

LANDSAT 7 ETM+		LANDSAT 8 OLI	
BANDS	**WAVELENGTHS (nm)**	**BANDS**	**WAVELENGTHS (nm)**
Band 1 - Blue	450 - 520	Band 1 - Coastal Aerosol	430 - 450
Band 2 - Green	520 - 600	Band 2 - Blue	450 - 510
Band 3 - Red	630 - 690	Band 3 - Green	530 - 590
Band 4 - Near Infrared	770 - 900	Band 4 - Red	640 - 670
Band 5 - SWIR 1	1550 - 1750	Band 5 - Near Infrared	850 - 880
Band 6 (Thermal)	10400 - 12500	Band 6 - SWIR 1	1570 - 1650
Band 7 - SWIR 2	2090 - 2035	Band 7 - SWIR 2	2110 - 2290
Band 8 (Panchromatic)	520 - 900	Band 8 - Panchromatic	500 - 1380
		Band 9 - Cirrus	1360 - 1380
		Band 10 - TIRS 1	10600 - 11190
		Band 11 - TIRS 2	1150 - 12510

Ground Truth Data

According to the method suggested by Hall et al. (1991), 50 study points in total were chosen with a homogeneous groundcover of *E. nigrum*. Ground truth data were collected from dispersed locations between the coastal islands towards the continental areas of Skibotn in Troms county (Figure 5A), as well as on the Ifjord mountain areas in Finnmark county (Figure 5B). Study points were selected to include areas with different degree of *E. nigrum* cover where the abundances of *E. nigrum* vary between 10-100 per cent. Each point was registered by UTM coordinates in the centre (Hall et

al., 1991) of a square representing the pixel size of the remote sensing data and aligning the square in the North-South direction.

Considering the pixel resolution of Landsat data (30 x 30 m), the location of each point was selected, within a flat, larger homogeneous area in order to account for georeferencing errors in the satellite data. The size of each field sampling location was 40 x 40 meter, slightly larger than the size of the Landsat image pixel (30 x 30 meter) (Kerr and Ostrovsky, 2003). For every meter, either the presence or the absence of *E. nigrum* was recorded. For every study point, a total of 280 recordings were made. Finally, the data recorded from the field were transferred and collected in an Excel file (APPENDIX III).

Remote Sensing Analyses

The reflected radiation from a pixel, as recorded in remote sensing imagery, has rarely interacted with a volume composed of a single homogeneous material, because natural surfaces composed of a single uniform material do not exist in nature. Usually, the electromagnetic radiation observed as pixel reflectance values results from the spectral mixture of a number of ground spectral classes present at the surface sensed. (Van Der Meer and De Jong, 1999, Van Der Meer, 1995). This means that *E. nigrum* reflectance value does not appear as a single reflectance value in a pixel, but as mixture reflectance spectrum of several compounds that appear in that pixel, such as coexistence species.

The software used for the study was ENVI (ENVI, 2004), an image processing system. The first step made in the scenes analyses was to extract a subset of the Landsat scene containing regions that includes the two different study areas (Figure 6 and 7). Moreover, both Coastal aerosol band and Cirrus band in Landsat 8 OLI were ignored due to the lack of relevant information for the project.

Every different preprocessing (raw image data, radiometric correction, masking) and all different classification approaches were tried in Ifjord area subset image at first, before determining which one would be the best method to use. The methods achieving the most accurate result were chosen to be applied in the Tromsø study area (spectral unmixing on the radiometric corrected area) (Figure 2).

Figure 6. A subset of the Landsat 8 OLI sensor covering the Ifjord study area (path 194, row 10).

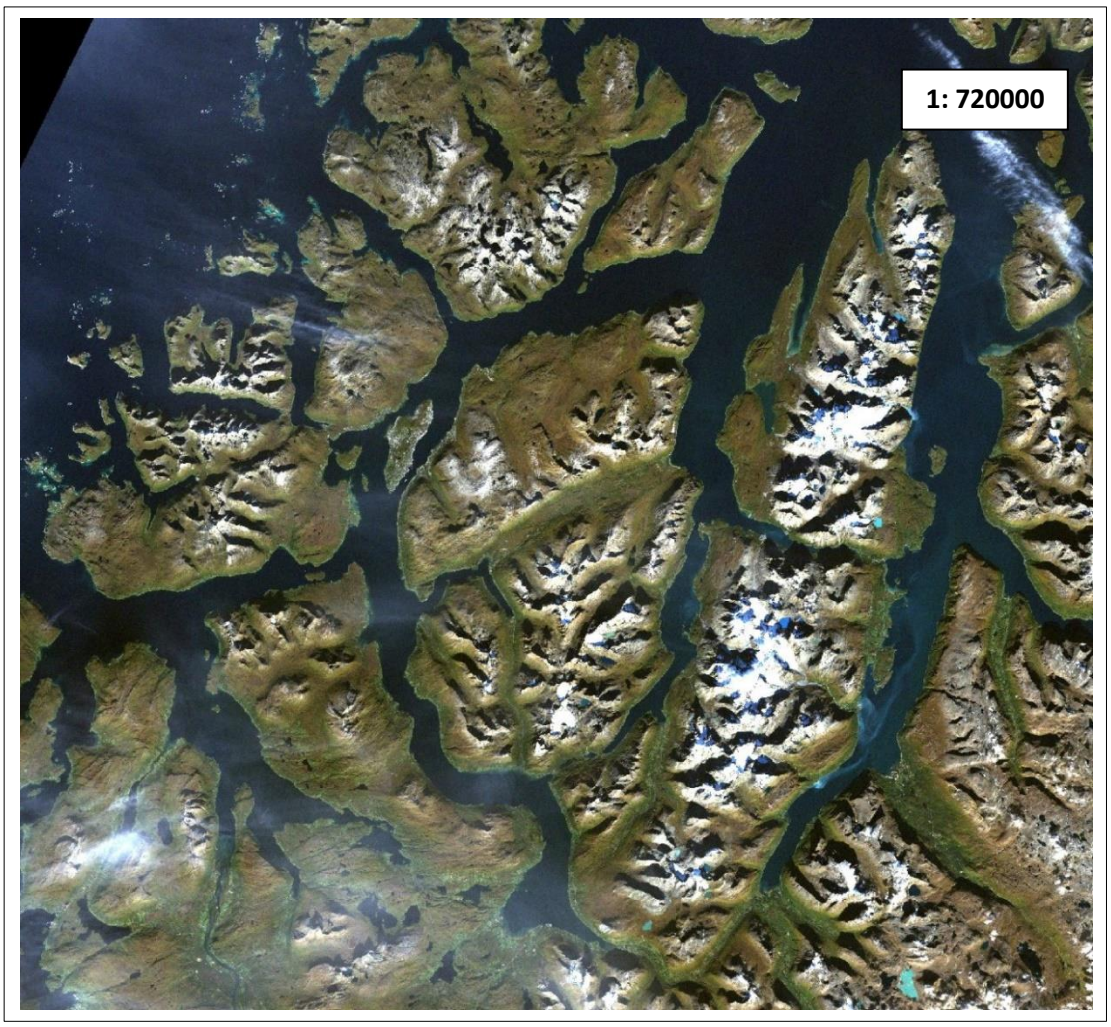

Figure 7. A subset of the Landsat ETM+ 7 sensor covering the Tromsø study area (path 197, row 11).

The next phase was to find out which classification method would be the best for the study. Classification took place on three levels of preprocessed satellite data: raw image (no preprocessing), radiometric corrected image and radiometric corrected and masked image (Figure 2).

First, in the raw Landsat 8 OLI image, the endmember determination and the different classification methods were tried. In the case of endmember determination, the set of

distinct spectra that constitute the mixed pixels in the scene was estimated (Keshava and Mustard, 2002). Selection of endmembers can be achieved in two ways (Van Der Meer and De Jong, 1999, Keshava and Mustard, 2002), (1) deriving endmembers from the purest pixels in the image, or (2) selecting endmembers from spectral (field or laboratory) library.

Then, a radiometric correction was performed in each image where the classifications algorithms were performed again. Radiometric correction of remote sensing data usually involves the process of correcting radiometric errors or distortions of digital images (Xie et al., 2008, Hall et al., 1991). An absolute reflectance of the scene objects was extracted, requiring an input of simultaneous atmospheric properties and sensor calibration found in Metadata file (Franklin and Wulder, 2002, Xie et al., 2008).

Finally, a mask was created in the radiometric corrected image. Masking is used to eliminate areas of no interest in an image. A mask is a binary image that consists of values of 0 and 1. When a mask is used in a processing function, the areas with values of 1 are processed and the masked 0 values are not included in the calculations [see more (ENVI, 2004)].

Several analyses were done in order to extract and analyse the cover of *E. nigrum* (Hall et al., 1991). Traditional classification methods were used such as supervised (Spectral Unmixing and Maximum Likelihood classification) and unsupervised classification methods (Isodata and K-Means).

Xie et al. (2008) defines supervised classification as "learning an established classification from a training set, which contains the predictor variables measured in each sampling unit and assigns prior classes to the sampling units".

Spectral unmixing is a technique in which the measured spectrum of a mixed pixel is decomposed into a number of spectral components, or endmembers, and a set of corresponding fractions, or abundances, that indicate the proportion of each endmember present in the image pixel (Van Der Meer, 1995, Van Der Meer and De Jong, 1999, Keshava and Mustard, 2002). It assumes linearity, i.e. the individual component reflectance is multiplied by their relative proportional amounts (Equation 1).

$$Ri = \sum_{j=1}^{n} f\ j\ Re\ ij\ +\ \varepsilon\ \mathrm{j} \qquad \text{(Equation 1)}$$

R_i = reflectance of the mixed spectrum of a pixel in image band *i*

f_j = fraction endmember *j* ('abundance')

Re_{ij} = reflectance of the endmember spectrum *j* in band *i*

ε_j = the residual error (difference between the measured and modelled digital number (DN) in band *i*.

n = number of endmembers

Constraining assumptions:

$$\sum_{j=1}^{n} f\ j\ = 1 \qquad 0 < 0 < f_j \leq 1$$

The result is an abundance image for each endmember in the mixing model giving the relative abundance of a component at every pixel (Van Der Meer, 1995, ENVI, 2004). The error image results from the difference between the observed pixel spectrum and the spectrum reconstructed from the calculated abundances. It displays how well the mixing library can be used to model each observed spectrum.

In the case of Maximum Likelihood, it assumes that the statistics for each band class are normally distributed and calculates probability that a given pixel belongs to a specific class (ENVI, 2004, Richards and Jia, 1999).

On the other hand, unsupervised classification (K-Means and Isodata) relies on spectrally pixel-based statistics and incorporates no prior knowledge of the characteristics of the themes being studied. They calculate initial class means evenly distributed in the data space and then iteratively clusters the pixels into de nearest class using a minimum distance technique. Isodata unsupervised classification calculates class means evenly distributed in the data space, and then, iteratively clusters the remaining pixels using minimum distance techniques. Whereas, K-means unsupervised classification calculates initial class means evenly distributed in the data space and then iteratively clusters the pixels into the nearest class using a minimum distance techniques [see more (ENVI, 2004)].

However, it is hard to obtain precise classification results using them. The reasons are that the same vegetation type on ground may have different spectral features in remote sensed images and additionally, different vegetation types may possess similar spectra. Due to these reasons, improved classifiers were executed such as Neural Net classification and Spectral Angle Mapper. They are very useful in extracting vegetation-type information in complex vegetation mapping problem (Xie et al., 2008).

Neural Net Classification and Spectral Angle Mapper were performed. Neural Net classification can be computationally demanding when large datasets dealt to train the network and sometimes no result may be achieved at all even after a long-time computation due to local minimum [see more (Xie et al., 2008, ENVI, 2004, Richards and Jia, 1999, Rumelhart et al., 1988)]. Spectral Angle Mapper (Xie et al., 2008, ENVI,

2004) identifies the distance between pairs of signatures for classification. It is a physically-based spectral classification that uses an *n*-dimensional angle, where *n* is the number of bands, to match pixels to reference spectra. It is run on reflectance data and it is independent of a multiplicative factor, since it only uses the direction of the vector (i.e. the angle), not the vector's length. A rule image is produced per endmember showing the spectral angle for each pixel spectrum per endmember.

Statistical Analyses

Descriptive statistics of field abundance estimation and *E. nigru*m abundance extraction from the spectral unmixing were performed (mean, variance, standard deviation and range). Pearson correlation test was used in both areas combined as well as in Ifjord and in Tromsø area separately. They were plotted where the predictor value was the field abundance estimation of *E. nigrum*. Additionally, residual errors were calculated and plotted. Each model was conducted in both areas together and in each area separately using R (R_Development_Core_Team, 2013).

Some study points of the Tromsø study area were not used in the statistical analyses because they are either shaded or snowed areas (1209_02, 1209_03, 1209_12, 1209_13, 1209_17) in the image as well as outliers (1209_05, 1306_31).

Finally, logarithmic transformation was made in order to force both of the scales to become linear in the correlation plot between 'Field Abundance estimation' of *E. nigrum* and *E. nigrum* 'Abundance extraction' from the spectral unmixing.

PROCESS AND RESULTS

ASD FieldSpec Analyses

Regarding with the Batatasin-III calibration using ASD FieldSpec spectroradiomenter, the preliminary results in R showed an r of 0.81 with a p value < 0.01.Thus, ASD FieldSpec spectroradiometer can be used as an analytical quantitative tool for Batatasin-III concentrations in *E. nigrum* leaves (Figure 8) (APPENDIX II). It confirmed Batatasin-III could potentially be measured through remote sensing image data, i.e. Landsat satellite images.

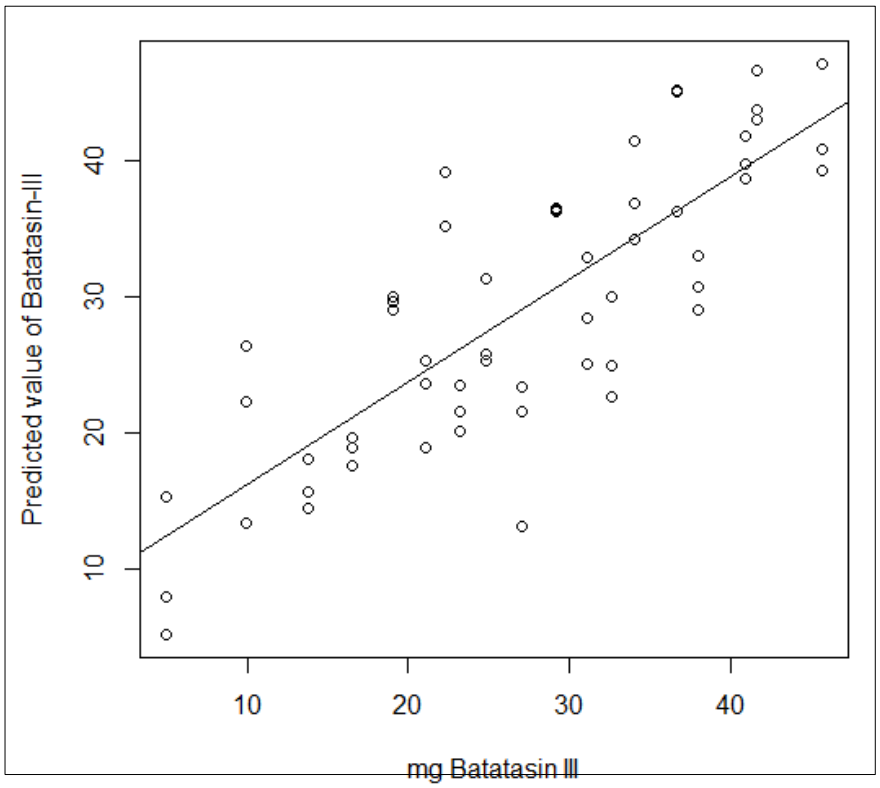

Figure 8. Batatasin-III calibration with ASD FieldSpec spectrometer. Predicted value of Batatasin-III (y axis) against measured values of Batatasin-III by HPLC technique (x axis).

Regarding with the ASD FieldSpec measurements in the field and its predicted value of Batatasin III in their leaves, it is obtained r (Pearson correlation coefficient) of 0.15. The

result showed that the *E. nigrum* coverage in field is not dependent with the abundance of Batatasin-III (Figure 9).

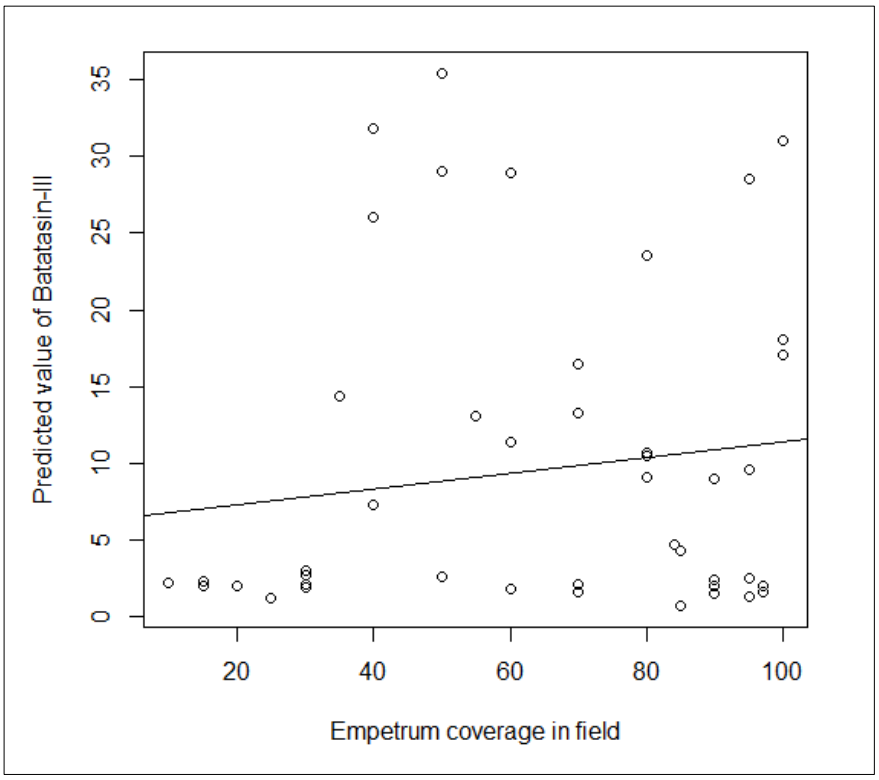

Figure 9. *Empetrum nigrum* coverage in Tromsøya, Lyfjord and Rebbenesøya field plots (x axis). Batatasin-III predicted value from the validation made with ASD FieldSpec spectroradiometer (y axis).

Ifjord Area Analyses

For a better comprehension, this part will be divided in the different steps that were followed to find out which method was going to be used.

1. Raw Image Data

1.1. Supervised Classification

1.1.1. Spectral Unmixing

First, spectral unmixing is performed. In the raw Landsat image, an endmember determination was made.

As the simplest spectral unmixing, three endmembers were taken, 'Empetrum presence' 'water' and 'clouds' (Figure 2 and Table 2, Spectral Unmixing 1). In ENVI, it is necessary to create vector layers of each endmember. For 'Empetrum presence', pixels with high *E. nigrum* coverage were selected. They were corresponded to those georeferenced pixels in which study points with higher *E. nigrum* coverage were placed, i.e. 1306_34: 97.50%; 1306_43: 97.50%; 1306_46: 98.33%. In the case of 'water' and 'clouds' vector layer, *Spectral Profile* tool was used in order to check each endmember spectral signature. Thus, it was possible to verify the selected pixels for the vector layers corresponding with the spectral signature of such targets as well as to distinguish them in the scene due to the known area. Then, each vector layer was converted into Region Of Interests (ROI) with *Convert Vector to ROI* ENVI tool and created a Spectral Library with the ROIs or endmembers required. Spectral Unmixing is performed. A *unit sum constraint* of 0.003 was set as theory says that this value needs to be approximately 10 times larger than variances observed in certain channels (ENVI, 2004). The results of spectral unmixing appear as a series of grey-scale images, one for each endmember, i.e. 'Empetrum presence' 'water' and 'clouds', plus a root-mean-square (RMS) error image. Higher abundances (and higher errors for the RMS error image) are represented by brighter pixels. The results are dependent on the input endmembers and will change if the endmembers are changed (ENVI, 2004). In RMS error image, the better spectral

unmixing, the lesser geometric pattern in the image. The final step was to extract the values of each study point in digital numbers from 'Empetrum presence' image. In this part, ArcGIS (geographic information) system was used (Johnston et al., 2001). A simple correlation was made calculating its R^2 between percentage of *E. nigrum* abundance extracted by the spectral unmixing (value 255 in digital numbers correspond to 100%) and the percentage of *E. nigrum* abundance in field (ground truth data).

As it was written previously, the results are dependent on the endmembers. Therefore, more endmembers were added for improving the results, i.e. 'Empetrum presence' 'water', 'clouds', 'background' (bare soil and rock) and 'roads' (Figure 2 and Table 2, Spectral Unmixing 2). Every endmember was selected as before including the new endmembers, 'background' and 'roads', which were selected as 'water' and 'clouds' endmembers. The following steps were done in the same way as in the first spectral unmixing made.

1.1.2. Maximum Likelihood Classification

Before executing any Maximum Likelihood classification, it is necessary to collect endmembers. Endmembers of 'water', 'road', 'clouds', 'background' and 'vegetation' were compiled as in Spectral Unmixing 2, and used (Figure 2 and Table 2, Maximum Likelihood 1). The probability threshold was set as 0.25, this means pixels with probabilities lower than 0.25 will not be classified (ENVI, 2004). Next step was to use *Classification to vector* tool in ENVI for creating a new vegetation vector layer and use it as ROI. Then, a class image from vegetation ROI is created. It is possible to use that vegetation class image and make the spectral unmixing using two endmembers, 'Empetrum presence' and 'Empetrum absence'. For 'Empetrum presence', pixels were selected as in the first spectral unmixing. However, for 'Empetrum absence', pixels with

high grasses abundance were selected. It was a trivial case because the pixels were selected regarding the knowledge of the study area and using *Spectral Profile* tool. Then, they were compared with a normal vegetation spectrum (Figure 1).

1.2. Unsupervised Classification

For unsupervised classification, Isodata and K-means algorithms were used. Once the unsupervised classifications were done, which of the classes belongs to the vegetation class was decided. Afterwards, as in Maximum Likelihood Classification, 'water', 'roads' and 'background' endmembers were collected. However, the vegetation class obtained in the unsupervised classification was taken as 'vegetation' endmember. Finally, new spectral unmixing was performed (Figure 2 and Table 2, Isodata 1 and K-Means)

2. Radiometric Correction

Radiometric correction was performed in order to correct radiometric errors in the images.

2.1. Supervised Classification

2.1.1. Spectral Unmixing

Endmembers from spectral (field or laboratory) library were selected (Van Der Meer and De Jong, 1999, Keshava and Mustard, 2002). For this, spectra from ASD FieldSpec were used. The goal was to create new spectral libraries, one spectral library with ASD Fieldspec data from field measurements and add endmembers such as 'clouds', 'roads' and 'water' to each one (Figure 2 and Table 2, ASD Data 1). It was necessary to convolve ASD Fieldspec data into Landsat data. *Spectral Library Resampling* tool can convert ASD Fieldspec data into a Landsat format with the option *Predefine filter*

function. In addition, a radiometric correction was necessary to convert Landsat dataset into reflectance values as ASD FieldSpec dataset.

ENVI software is also used in this step. *Apply Gain and Offset* tool is performed to apply a simple gain and offset correction to a set of bands. ENVI multiplies the selected bands by an input gain value and adds a predefined offset value (ENVI, 2004). Moreover, *Dark Substraction* (Franklin and Wulder, 2002, ENVI, 2004) is made to apply atmospheric scattering correction to the image and reduce atmospheric effects in the scene. The result is an image in scaled reflectance values. Once that radiometric correction is done, the spectral library can be created for running another spectral unmixing.

Having improved the image with a radiometric correction, new classifications and spectral unmixings were done. First, three different spectral unmixings taken as endmembers, (1) 'background', 'Empetrum absence' (grasses) and 'Empetrum presence' (Figure 2 and Table 2, Spectral Unmixing 3; Figure 10); (2) 'background', 'roads', 'clouds', 'water', 'Empetrum absence' and 'Empetrum presence' (Figure 2 and Table 2, Spectral Unmixing 4); (3) 'background', 'roads', 'clouds', 'water', 'Empetrum absence', 'Empetrum_70-75%', 'Empetrum_75-80%', 'Empetrum_80-86%', 'Empetrum_89-91%', 'Empetrum_91-95%' and 'Empetrum_95-100%' (Figure 2 and Table 2, Spectral Unmixing 5). Here, a complete endmember determination was tried to get the better result in the *E. nigrum* cover extraction. Second, spectra from the ASD Fieldspec spectral library were selected, one with 100% of *E. nigrum*, Reb01, and another with the lowest percentage of *E. nigrum* in field, Tro54 (Figure 2 and Table 2, ASD Data 2).

2.1.2. Maximum Likelihood Classification

In the case of the Maximum Likelihood classification (Figure 2 and Table 2, Maximum Likelihood 2), with new endmembers determination, i.e. 'background', 'roads', 'clouds', 'water', 'Empetrum absence' and 'Empetrum presence' the algorithm was run after the radiometric correction. However, in the case of 'Empetrum presence' endmember, the program requires a minimum number of pixels selected for creating a new endmember. Therefore, not only the pixels representing the study point with the higher abundances were taken (1306_34: 97.50%; 1306_43: 97.50%; 1306_46: 98.33) but some pixels surrounding the study point pixel. These pixels coincide with the pixels taken in the raw image.

2.2. Unsupervised Classification

Unsupervised classifications (Figure 2 and Table 2, Isodata 2 and K-Means 2), were performed again with the radiometric corrected image.

2.3. Neural Net Classification

For the Neural Net classification (Figure 2 and Table 2, Neural Net), six vector layers were created, i.e. 'background', 'roads', 'clouds', 'water', 'Empetrum absence' and 'Empetrum presence'. Then ROIs were made from the vector layers for a new spectral library. *Neural Net Classification* was performed in ENVI and Default settings were used. The result in Neural Net classification is a rule image from each endmember and a RMS error image.

2.4. Spectral Angle Mapper

A spectral library with Batatasin-III absorbance data from Zbynek was created. Endmembers were 'Batatasin-III', 'Ficus leaf' and 'Batatasin-III+Ficus leaf'. Spectral Angle Mapper classifier (Figure 2 and Table 2, Spectral Angle Mapper) was performed

using the new spectral library. The purpose of executing this method was to determine whether Batatasin-III was observable as *E. nigrum* feature by remote sensing or not. However, it resulted in a complete black image from the Batatasin-III endmember indicating that Batatasin-III cannot be extracted from the image.

3. Masking

Masking was tried as a final step for improving the results in the spectral unmixing. From Isodata unsupervised classification, classes that are not vegetation were reclassified to 0 such as water, roads and clouds and vegetation to 1.

3.1. Supervised Classification

3.1.1. Spectral Unmixing

With a radiometric corrected and masked image, new spectral unmixings were tried. (1) Spectral unmixing where the endmembers selected were 'background', 'Empetrum presence', 'Empetrum absence' (Figure 2 and Table 2, Spectra Unmixing 6); another (2) spectral unmixing in which the spectra from the ASD Fieldspec spectral library were selected with the highest and the lowest *E. nigrum* cover in field (Figure 2 and Table 2, ASD Data 3).

3.1.2. Maximum Likelihood Classification

'Empetrum presence', 'Empetrum absence' (grasses) and 'background' were selected as endmembers for the Maximum Likelihood classification (Figure 2 and Table 2, Maximum Likelihood 3).

3.2. Unsupervised Classification

Unsupervised (Figure 2 and Table 2, Isodata 3 and K-Means 3) classifications were performed after making a radiometric correction and masking in the image.

Once the different methods were performed, R^2 calculated in Excel in each different classification method (Table 2) were compared in order to identify which steps were needed to get a better result. The same steps were made in the Tromsø scene.

Table 2. Steps followed with the different remote sensing classification methods and its R^2.

Steps	Classification method	R^2
Raw Image Data	Spectral Unmixing 1	0,00
	Spectral Unmixing 2	0,00
	Maximum Likelihood 1	0,01
	Isodata 1	0,04
	K-Means 1	0,04
Radiometric Corrected Data	ASD Data 1	0,04
	Spectral Unmixing 3	0,05
	Spectral Unmixing 4	0,32
	Spectral Unmixing 5	0,00
	ASD Data 2	0,04
	Maximum Likelihood 2	0,01
	Isodata 2	-
	K-Means 2	-
	Neural Net	0,12
	Spectral Angle Mapper	-
Masked Data	Spectral Unmixing 6	0,04
	ASD Data 3	0,03
	Maximum Likelihood 3	-
	Isodata 3	-
	K-Means 3	-

Tromsø Area Analyses

The first step was to perform a radiometric correction as in the Ifjord scene. The best result obtained in Ifjord image occurred when carrying out a spectral unmixing (Spectral Unmixing 4, see Table 2) determining 'background', 'roads', 'clouds', 'water', 'Empetrum absence' and 'Empetrum presence' as endmembers (Figure 10). In Tromsø image, the endmembers determination was more difficult than in the Ifjord area. One of the reasons was that the subset region was larger than in Ifjord region. To ease the task,

the image was virtually divided in smaller areas surrounding the study points and the endmembers determination was made depending on these virtual areas, i.e. Kvaløya_Sommarøy, Kavaløya_Tromsø_Håkøya, Kvaløvågen_Risvik_Lyfjord, Rebennes_Skogfjord_Hansnes, Road91_Svensy, Skibotn_Kilpis (Figure 11).

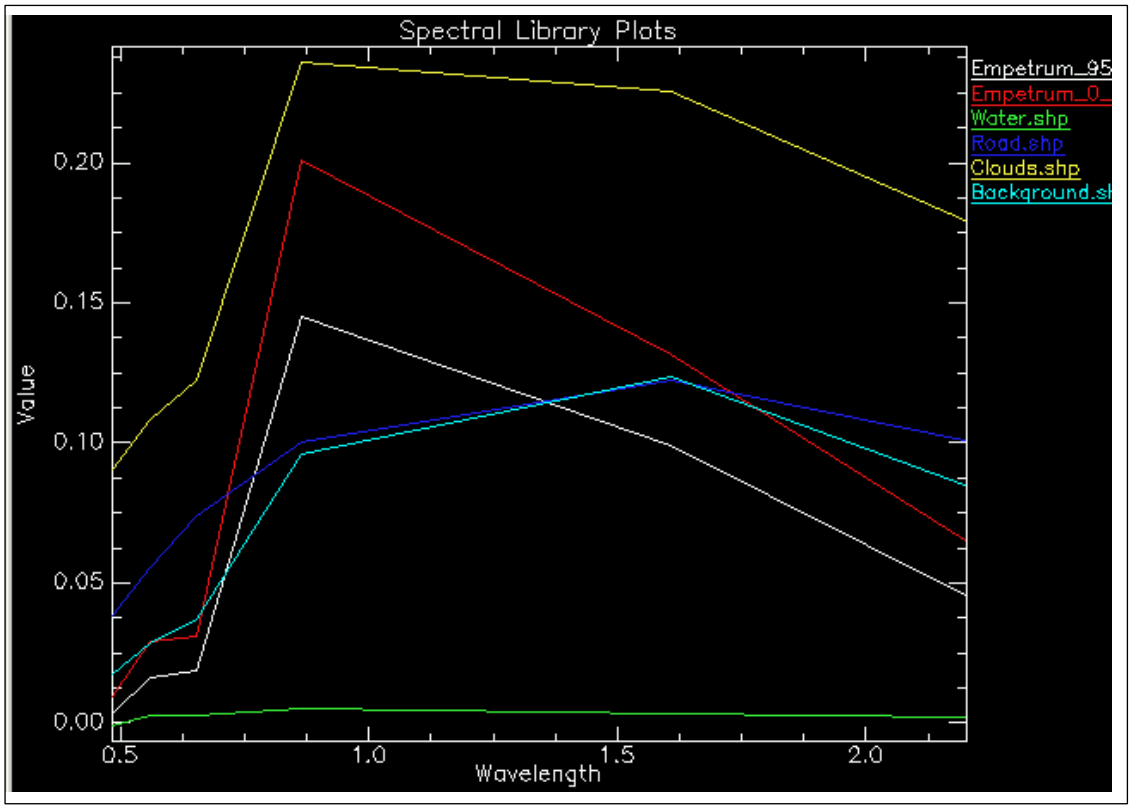

Figure 10. Endmembers collection from Ifjord Area used in Spectral Unmixing 4. X axis is the wavelength in micrometer and Y axis is the reflectance values in percentage.

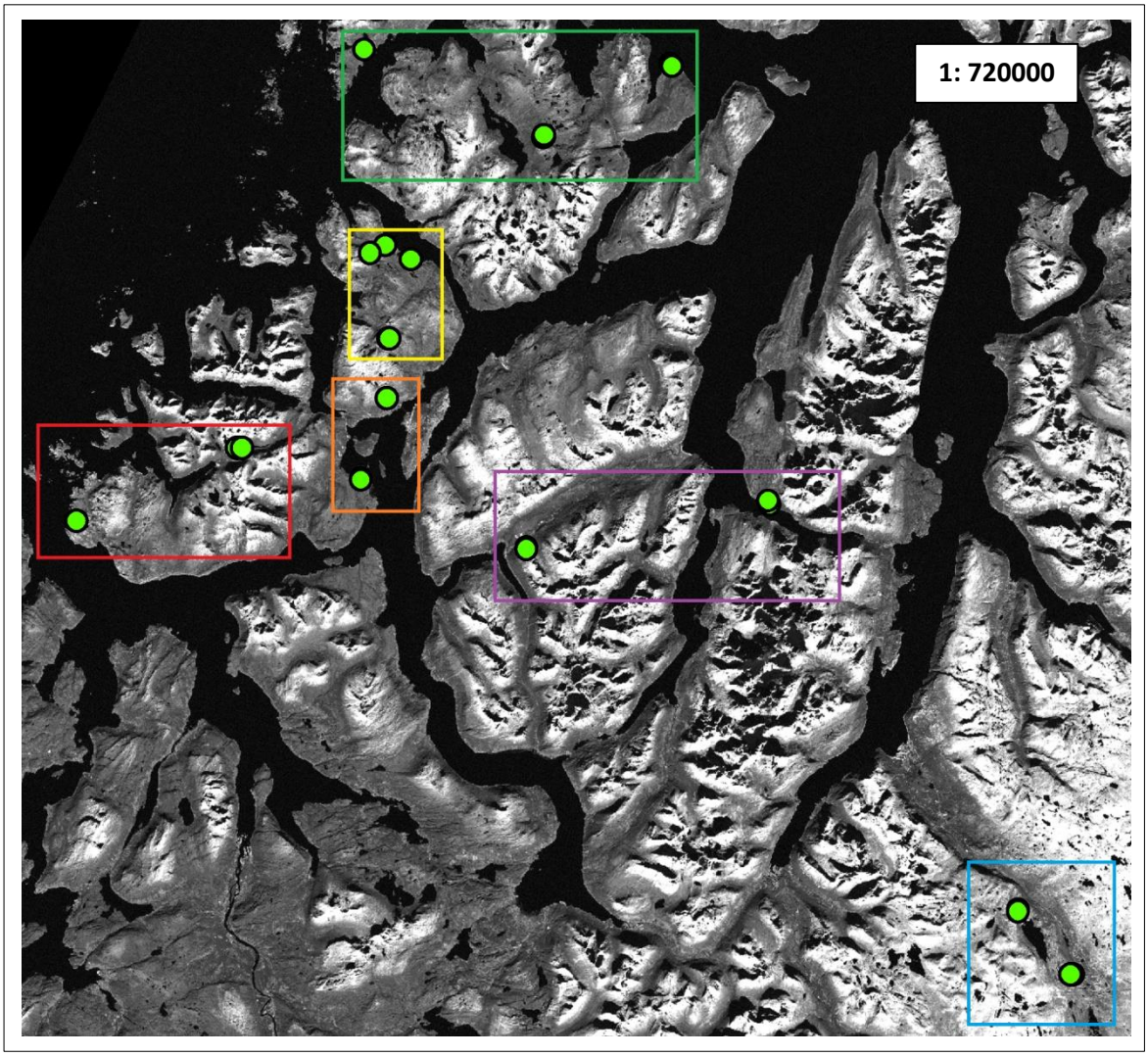

Figure 11. Troms area and endmembers selection areas. Kvaløya_Sommarøy (red); Kavaløya_Tromsø_Håkøya (orange); Kvaløvågen_Risvik_Lyfjord (yellow); Rebennes_Skogfjord_Hansnes (green); Road91_Svensy (purple); Skibotn_Kilpis (blue).

Endmembers were selected in the same way as in the Ifjord image. The result was a spectral library with several endmembers of the same classes, i.e. several endmembers covering water class. Hence, endmembers selected in Tromsø were 'water and shadows', 'forest', 'clouds', background', 'snow and clouds', 'grasses and forest', 'clouds and snow', 'grasses', 'clouds and urban' and 'Empetrum presence' (Figure 12). For 'Empetrum presence' endmember, pixels with high *E. nigrum* abundance were

selected as in Ifjord area. Those pixels were corresponding to some study points with the higher *E. nigrum* abundance determined by the ground truth data. Due to the large subset region taken in Tromsø scene, more ground study points were selected than in Ifjord (1209_01, 1209_03, 1209_04, 1209_05, 1209_06, 1209_07, 1209_08, 1209_09, 1209_10, 1209_11, 1209_14, 1209_15, 1209_16, 1209_18, 1209_19, 1209_20, 1209_21 and 1209_22). Seven study points were not taken into account because there was either a cloud or a shade area where the study point was placed. Finally, the same steps as in Ifjord area were done, setting the *unit sum constraint* as 3800 because, as it was explained in Ifjord Analyses section, the theory says that this value needs to be approximately 10 time larger than the variances observed in certain channels (spectral bands) (ENVI, 2004).

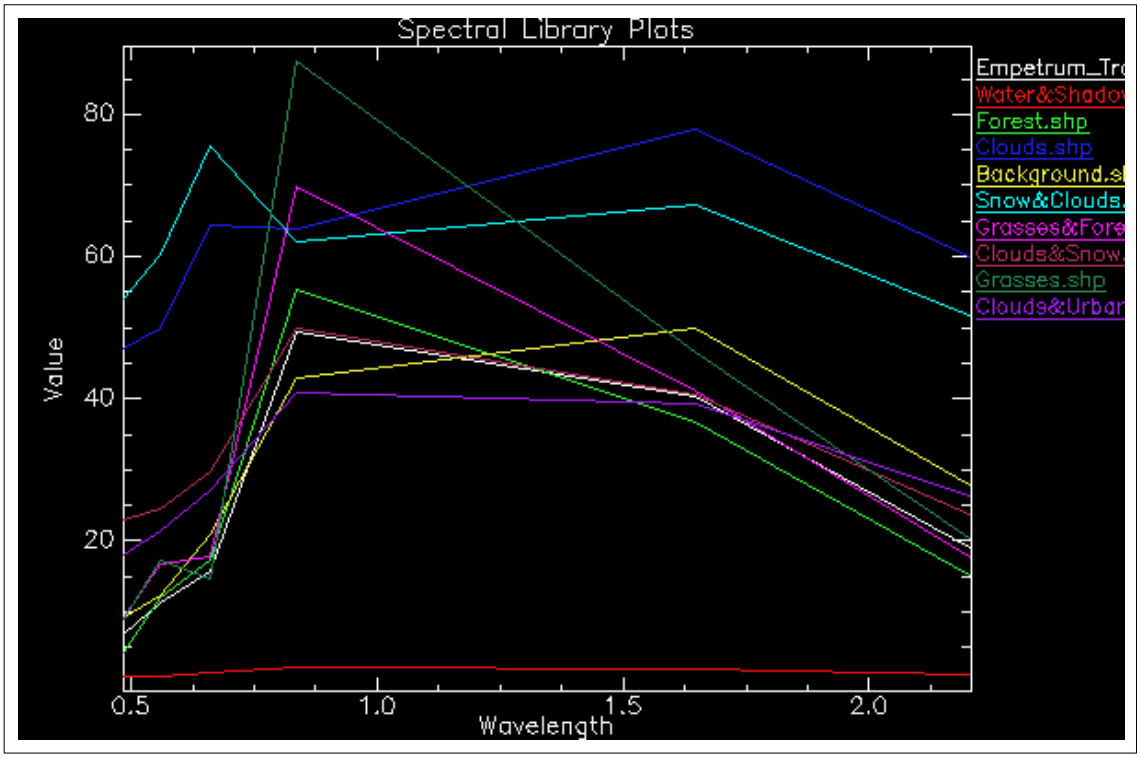

Figure 12. Spectral signature of endmember classes collection from Tromsø area. X axis is the wavelength in micrometer and Y axis is the reflectance values in percentage.

Images Results

Figure 13 and 14 show 'Empetrum presence' endmember image resulted from the spectral unmixing in both Ifjord and Tromsø area respectively. The lighter pixels represent the highest abundances of the endmember, whereas the darker pixels show the lowest abundances of the endmember (Van Der Meer, 1995), in this case *E. nigrum*. The values extracted from the image using ArcGIS in each image are shown in APPENDIX IV as well as the descriptive analysis for the Total area, Ifjord area and Tromsø area.

Pearson rank correlation coefficient test (r) between the field abundance estimation and the *E. nigrum* abundance extraction from the spectral unmixing of both study areas

combined results in a r of 0.15 and a p-value 0.35, being no significant ($p>0.05$) (Figure 15A). Analysing the two study areas separately, the Tromsø area achieved an r of 0.55 and a p-value 0.01 and in Ifjord area, the r is equal to 0.57 and its p-value ≤ 0.01 (Figure 15B and 15C). In Ifjord area and Tromsø area both p-values are less than 0.05 and a positive linear trend in observed in each plot.

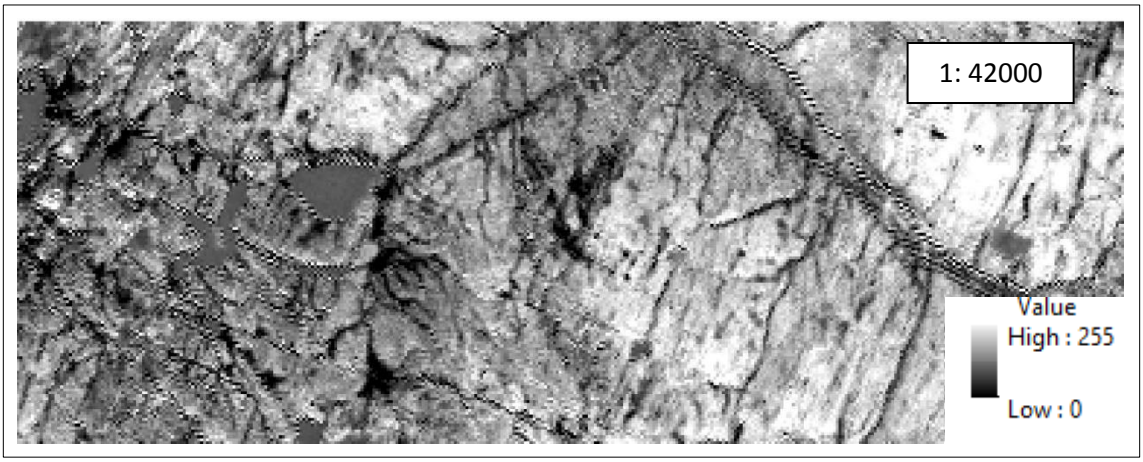

Figure 13. 'Empetrum presence' endmember image resulted from the spectral unmixing classification in the Ifjord study area. High: 255 is a 100% cover of *Empetrum nigrum* and Low: 0 is a 0% cover of *Empetrum nigrum*.

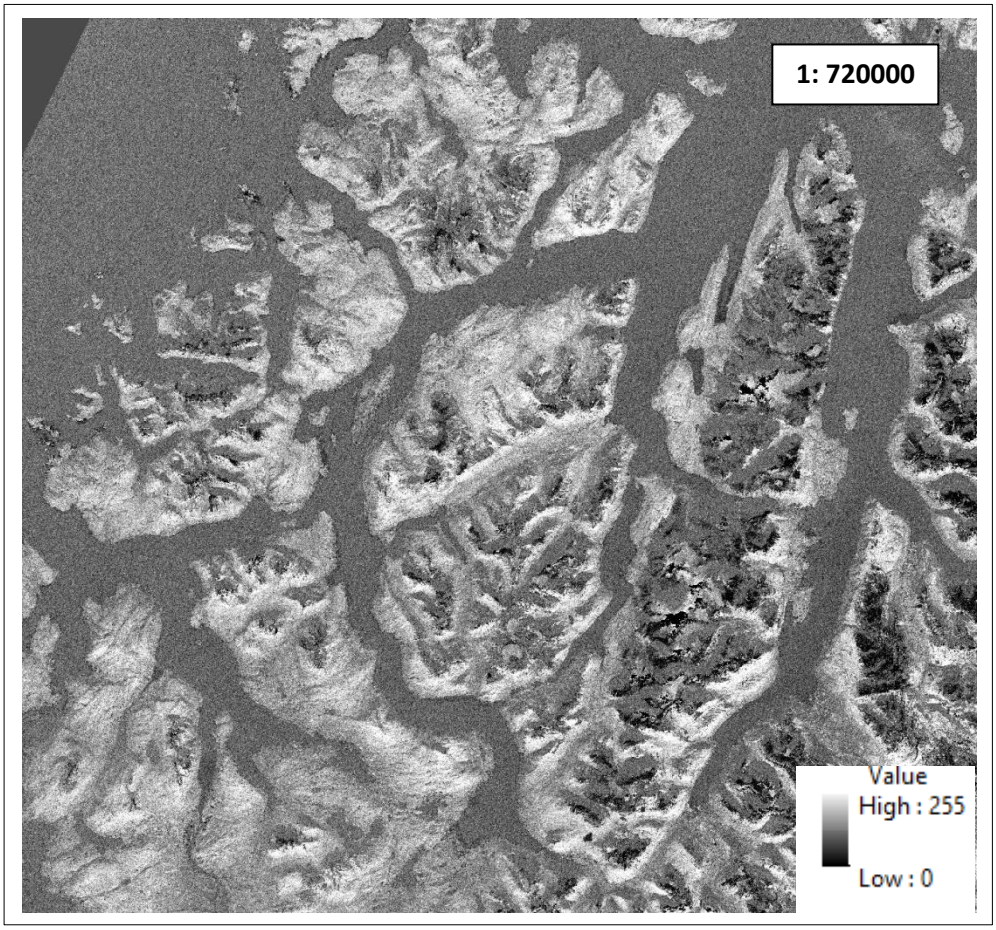

Figure 14. 'Empetrum presence' endmember image resulted from the spectral unmixing classification in the Tromsø study area. . High: 255 is a 100% cover of *Empetrum nigrum* and Low: 0 is a 0% cover of *Empetrum nigrum*.

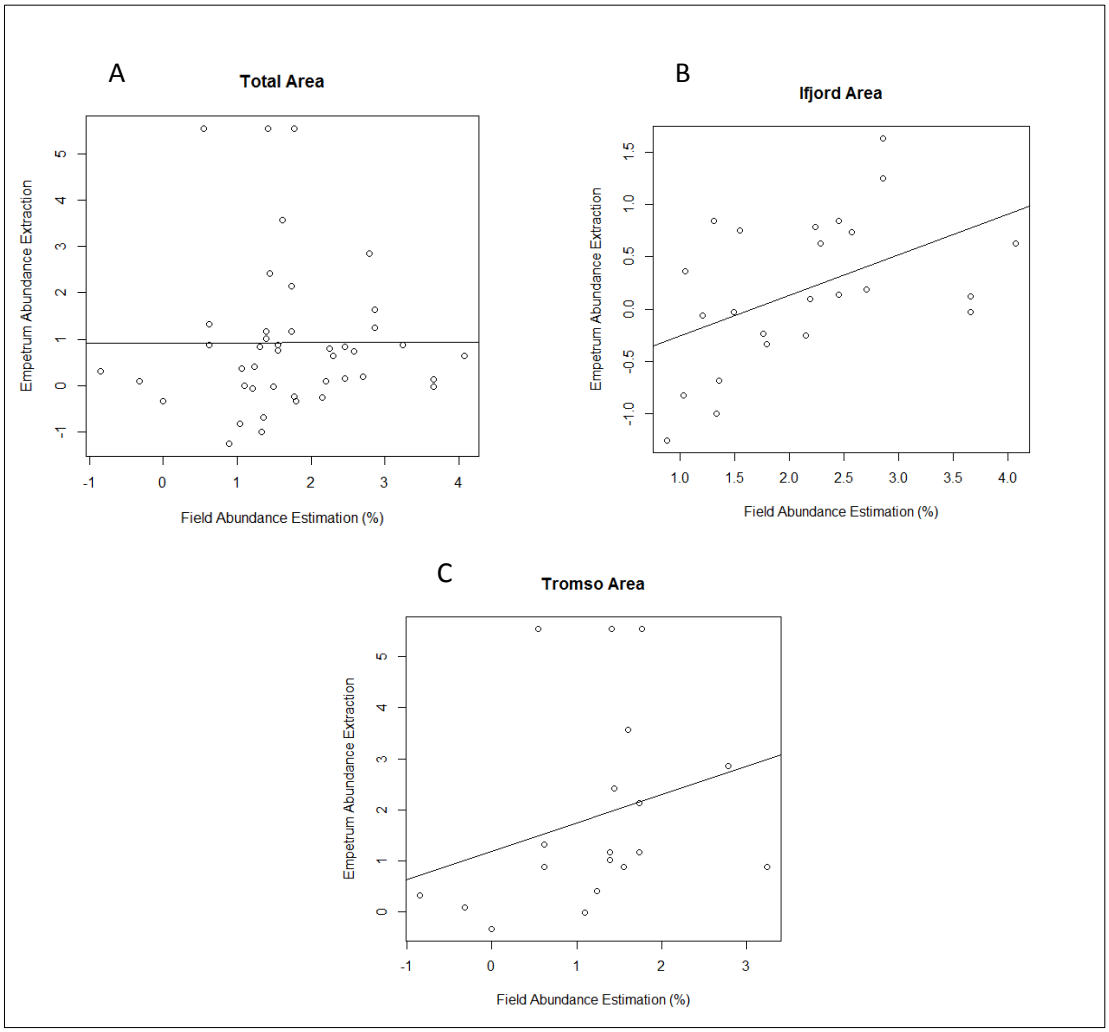

Figure 15. Correlation between field abundance estimation of Empetrum nigrum and spectral unmixing extraction of 'Empetrum presence' endmember (Logarithmic transformation) and trend line. A) Both study areas (Ifjord and Tromsø) combined. B) Ifjord study area. C) Tromsø study area

The residual error plots are shown in Figure 16A, B and C. Values are shown in APPENDIX V. Regarding the three plots, it can be observed that there is no pattern in none of the areas separately and in Total area.

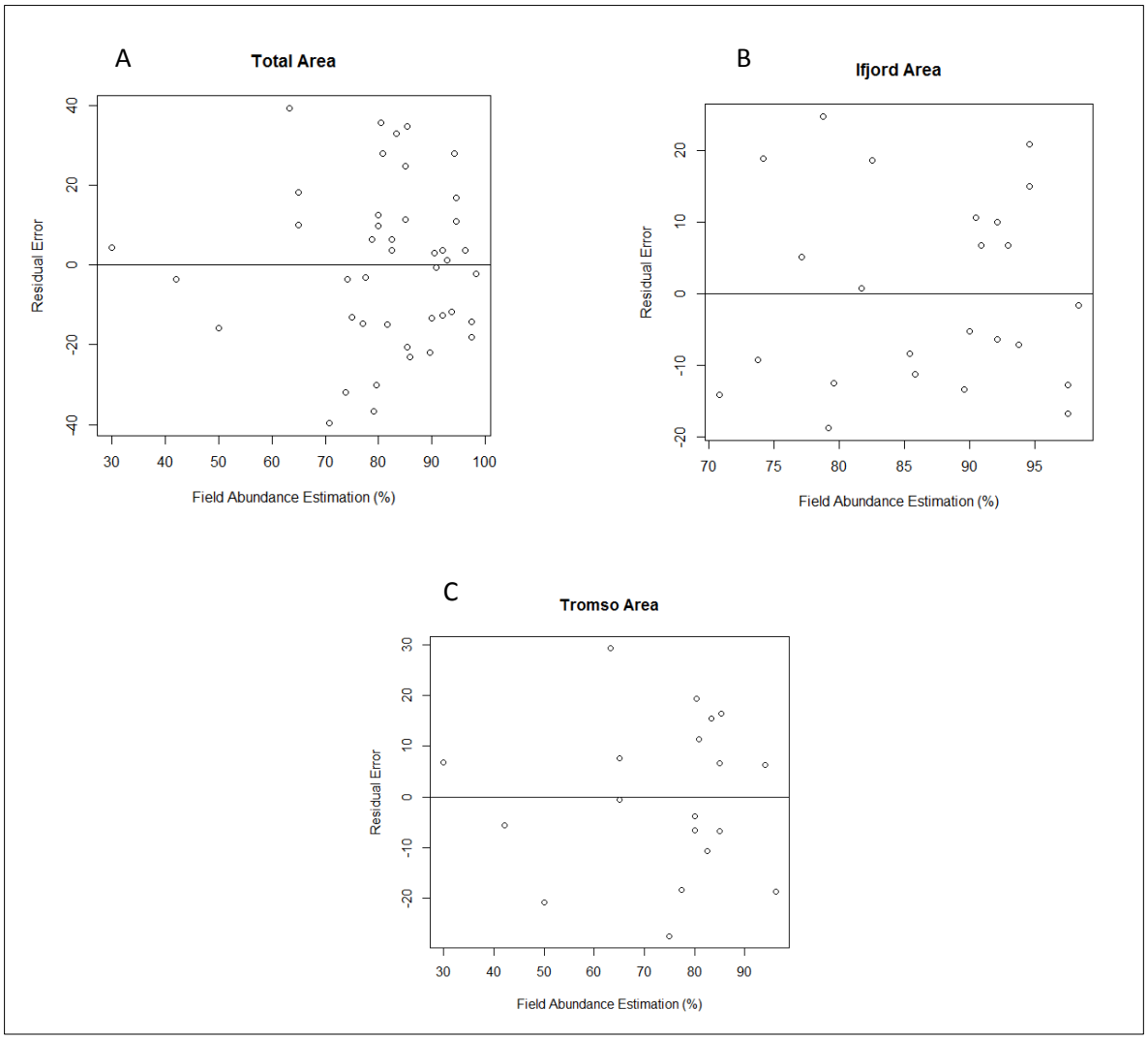

Figure 16. Residual error plot. X axis: field abundance estimation of E. nigrum in percentage. Y axis: residual error. A) Both study areas combined. B) Ifjord study area. C) Tromsø study area.

DISCUSSION

The aim of this study was to determinate how well different covers of *Empetrum nigrum* can be classified by means of remote sensing data. Thus, an *E. nigrum* spectral signature was required to create an accurate spectral library with not only *E. nigrum* classes but other predefined classes, or endmembers, found in the images. These endmembers were retrieved from the Landsat images. Moreover, a spectral library was created with ASD FieldSpec in the field. *E. nigrum* in coexistence with other common species was measured in order to create this spectral library.

Different supervised and unsupervised classification techniques were used for this aim. The best result was achieved when performing a spectral unmixing classification. The most accurate endmember determination was achieved in the spectral library when analysing the Ifjord and Tromsø areas separately. The correlation tests in both areas independently, determined not a perfect spectral unmixing of the endmembers, but good enough, r value of 0.57 in Ifjord and a r value of 0.55 in Tromsø, whereas in both areas combined, the r value was 0.15; knowing that several improvements, explained later in this section, could be done, i.e. imagery used, ancillary data, etc..

In the following a discussion on what might explain these low correlation coefficients is provided and a final section where some solutions are proposed for improving the spectral unmixing approach.

1. Endmember determination problem

The result of the spectral unmixing classification is highly dependent on the endmember determination (ENVI, 2004). As it is presented in results, Ifjord study area is smaller than Tromsø study area. Hence, endmembers that can be taken into account in Ifjord

area are fewer than those in Tromsø area, making it easier to include all of them in the spectral library. So, as it is shown previously, the spectral library in Tromsø has more endmembers than the spectral library in Ifjord.

Although Tromsø area has a higher number of endmembers in its spectral library, Ifjord classification is slightly more accurate with a higher correlation coefficient. One of the causes is related to the study area size in Tromsø, where there exists a challenge in covering all endmembers (classes). A lot of shaded areas and mixed targets on the image appear, i.e. clouds with urban areas, snow and clouds, shadows and snow, etc. as well as different types of rocks and vegetation that give different spectral signatures. This makes it more difficult to create a perfect spectral library with pure endmembers.

2. Spatial resolution problem

In the case of spatial scale or resolution, the question would be "could Landsat spatial resolution capture the cover variability of *E. nigrum* in field?" Cover variability of *E. nigrum* does not appear at 30 meters scale as the spatial resolution of Landsat. Although *E. nigrum* appears as homogeneous vegetation at this scale, being very dominant in arctic tundra (Tybirk et al., 2000, Bråthen et al., 2010), it appears in intimate coexistence with other vegetation such as *Betula nana*, *Vaccinum spp.*, graminoids and dichotyledons. This creates difficulties in distinguishing *E. nigrum* in the spectral unmixing classification. Theoretically, the spatial resolution of the image must be higher, hence the pixel size should be smaller than the size of the feature being classified to fully cover the classified objects (Domaç and Süzen, 2006), in this case, *E. nigrum*. Thus naturally mixed pixels as our study points, would always create problems and they will reduce to some extent the accuracy of classifications due to the spectral confusion they create (Domaç and Süzen, 2006). In case of the species studied, the

typical length-scale or gradient would be much more smaller (centimetres), since it co-habits with several shrub species (Tybirk et al., 2000), creating the difficulty to extract *E. nigrum* class or endmember by itself.

3. Temporal resolution problem

Regarding with temporal scales or resolution, the principal concern is the spectral variability of species features as a function of time. This was not taken into account in the study. There was a time frame to develop the field work, during September and June, avoiding the snowy period, regardless of the variability of species features. Moreover, not only the field work period but also, the image acquisition date, which is explained later on in "Data acquisition: Study points and imagery".

4. Spectral resolution problem

On the other hand, even though a significant but not strong correlation was achieved in each study areas separated, the spectral resolution is still an issue.

Landsat has low spectral resolution (Xie et al., 2008), i.e. 6 bands were used in the study. There are three bands covering the visible part where the chlorophyll feature appears. Nonetheless, there is a lack of bands for pigments and cell structure that appear in Near Infrared and Infrared part of the spectrum (Figure 1 and Table 1) (U.S Geological Survey, 2014). As it was written previously and several authors say (Domaç and Süzen, 2006, Xie et al., 2008), Landsat is often used to map vegetation at community level, e.g. forest, grasslands, etc. but not at species level.

Moreover, ancillary data with high spectral resolution, ASD FieldSpec spectra, was used to increase the accuracy of the classification (Aplin, 2004). The measurements made with ASD FieldSpec did not work when using them as endmembers for

performing the spectral unmixed classification. R^2 of 0.04 in ASD Data 1 and ASD Data 2 classifications, and R^2 of 0.03 in ASD Data 3 were obtained (Table 2). It is thought that the main reason was related to different study areas. Some common species existed, i.e. *Vaccinum myrtillus, Vaccinum uligonosum, Vaccinum vitis-idea, Arctostaphyllus alpina, Cornus suecica* and also graminoids, lichens, and bryophytes, but not all of them were shown in all areas, whereas, neither the association nor the coverage of these species was in coexistence with *E. nigrum* as in the ground truth study points. Besides, when the ASD FieldSpec measurements were taken, the weather was cloudy and rainy, and no radiometric correction was done afterwards.

5. Data acquisition: Study points and imagery

When doing basic biological research, there is usually a lack of information about how many study points are needed for the study, and the temptation may be either to use the biggest sample size that it can be afforded or a similar sample size as other researches (McDonald, 2009). During the field sampling period, the maximum number of study points possible were acquired, i.e. 50 study points, knowing that the general rule of thumb is no less than 50 study points for a correlation test (VanVoorhis and Morgan, 2007). Besides, the sampling was restricted by the snowy season.

The last problem is related to the imagery acquisition. Field work was carried out at different time than the acquisition of Landsat images, i.e. Ifjord scene is from August 2013 and Troms scene from September 1999. A significant feature for the large-area Landsat TM coverage problem is the use of imagery acquired at different times of the year or even in different years (Franklin and Wulder, 2002). Here, the temporal resolution problem appears again. The coverage and abundance of *E. nigrum* could have changed from 1999, despite its slow growing (Nilsson et al., 1998, Tybirk et al., 2000,

Elmendorf et al., 2012), as well as other disturbances in the ecosystem that could have occurred, e.g. new roads or paths. For solving this, the more images acquired the better discrimination. However, another problem appears, and it is to find image without clouds or shaded areas.

6. Solutions

Firstly, as Franklin and Wulder, 2002 said, "an ideal classification approach does not yet exist"; there might be a compromise within the information classes that are desired, the spectral information content of the imagery and the method used. Considering this, some ideas are given to solve the problems identified in this study.

Regarding the endmembers determination issue, several techniques were tried, (all of them explained in the methods on spectral analysis). Despite all of the different systems tried to acheive an accurate spectral library with the perfect endmembers in the laboratory, some could be better done in field. For instance, a better understanding of the area could be achieved. In the case of Ifjord, the study area was smaller, so the known area was relatively good. However, to determinate the endmembers in Tromsø area, virtual subareas were created (Figure 11), thus some classes could have been lost. This can be one of the reasons why the correlation coefficient is higher in Ifjord than in Tromsø.

Concerning the spatial resolution question, a spatial model is needed, establishing some rules about *E. nigrum* growth. For instance, it is known that *E. nigrum* is susceptible to fire, cutting, and trampling, and it does not have high sensitivity to acidification and/or eutrophication, tropospheric ozone, change UV:B radiation, global warming, or heavy metals as compared to coexisting species (Tybirk et al., 2000). Moreover, it is relatively resistant to environmental changes, but the long-term effect is not well known. Taking

into account these peculiarities of *E. nigrum*, a spatial model could be created. On the other hand, a Landsat peculiarity is its advantage in large areas studies (Xie et al., 2008, Reinke and Jones, 2006). In the case of ecosystems where *E. nigrum* is dominating, Landsat might not be suitable in every area though, i.e. uneven terrain with high changes in elevation, due to its spatial resolution. So, not only the dominance of *E. nigrum*, but the terrain, has to be taken into account when choosing the study area.

An improvement related to the temporal scale concern would be to perform a study of the variability of a specific feature of *E. nigrum*, i.e. evergreen feature, and the co-existence species throughout the growth study season. As an explanation, e.g. Figure 17, the arrow shows the highest spectral feature difference in a period of time and the circles represent no spectral difference between both species at that time. Hence, it will be possible to find the exact time of the year when the maximum difference between vegetation endmembers occur.

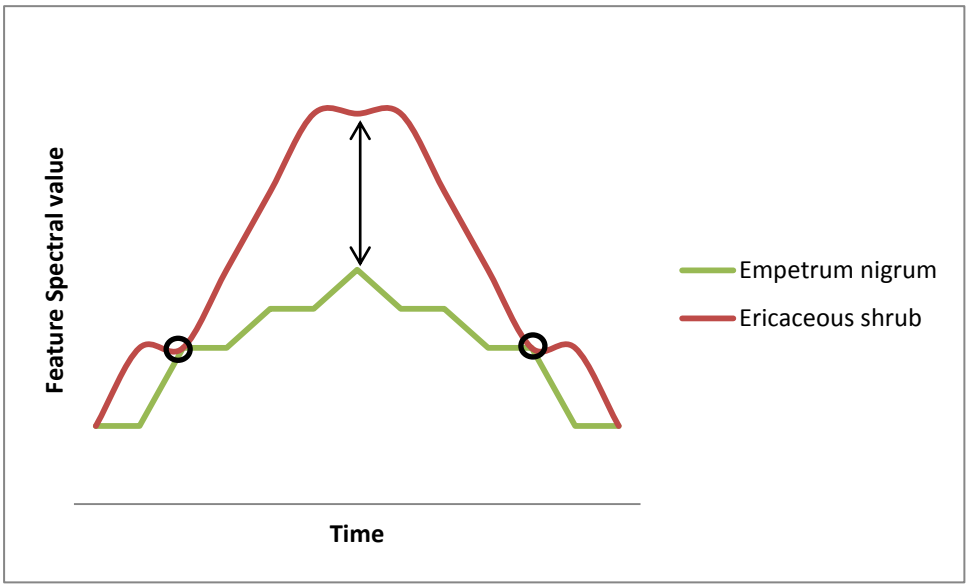

Figure 17. A theoretical example of spectral feature variability as a function of seasonal growth (time) of *Empetrum nigrum* and an ericaceous shrub species.

In the case of the spectral resolution problem, it was already explained the use of ancillary data with high spectral resolution (ASD FieldSpec spectroradiometer), to increase the classification accuracy. In the study, a specific signature of *E. nigrum* in field in coexistence with other common species of the habitat in Tromsøya, Lyfjord and Rebbenesøya was extracted. An improvement would be to have a spectral signature for *E. nigrum* and spectral signatures for each coexistence species. Moreover, taking the measurements in the same areas as the ground truth data would have been an advantage. In this way, a perfect spectral library could have been created.

So, both in temporal and spectral resolution issues, the solution would be the use of ASD FieldSpec spectrometer for measuring, not only *E. nigrum* spectral signature but coexisting species spectral signatures. Thus a temporal (seasonal) *E. nigrum* growth model is created as well as coexisting species growing models.

Finally, for solving the data acquisition problem, in the case of the study point, would be to have more time, thus more study points could be sampled. Regarding imagery acquisition, the more images acquisition, the better discrimination. However, it appears that the problem of finding images without clouds or shaded areas.

CONCLUSION

Endmembers determination was the key for *E. nigrum* classification. The spectral signatures of *E. nigrum* extracted from ASD FieldSpec spectroradiometer measurements in the laboratory were not satisfactory in order to use them in the classification. Thus, Landsat data were used to extract endmembers from the purest pixels, being one of them *E. nigrum* endmember, which has a specific spectral signature in Landsat images.

A spectral library was created with endmembers from the purest pixel in Landsat image, as well as, the spectral measurements taken with ASD FieldSpec. The most accurate spectral library used for the study was obtained through endmember determination from Landsat data. Then, the best result was achieved performing a spectral unmixing classification with such spectral library. The Pearson correlation tests between, the field abundance estimation of *E. nigrum* and the *E. nigrum* abundance estimation from this spectral unmixing classification, result in a r of 0.57 in Ifjord and a r of 0.55 in Tromsø.

Landsat is good option as a first attempt to determinate and classify *E. nigrum*. It is the only sensor that allows going back in time since 1972, it has good spatial cover, also at high latitudes and it is freely available data.

However, several improvements already explained can be done for getting an accurate spectral library and an accurate *E. nigrum* classification. These improvements are the previous study of the annual variability of *E. nigrum* and coexistence species, use of ancillary data and *E. nigrum* spatial model.

The opinion after developing this *E. nigrum* classification is that future studies need to include these improvements or solutions, in order to achieve an *E. nigrum* classification with a higher correlation coefficient from Landsat imagery.

ACKNOWLEDGEMENTS

I would like to express my deepest gratitude to my supervisors, Kari Anne Bråthen and Lennart Nilsen, for their advices and help during these two years, as well as for all the constructive comments to the previous versions of the thesis. Moreover, I would like to thank to all the people of Remote Sensing Laboratories of UZH for their warm welcome, especially to Michael Schaepman, for the guidance in this new world that remote sensing was for me. Lara and Anna Katherina, thank you for your great company and for lending a helping hand during the field work. Finally, I want to say thank you to my family and Asier, for their listening and their support everyday despite the distance, as well as my friends here in Tromsø and in Spain.

REFERENCES

APLIN, P. 2004. Remote sensing: land cover. *Progress in Physical Geography*, 28(2), pp. 283-293.

APLIN, P. 2005. Remote sensing: ecology. *Progress in Physical Geography*, 29(1), pp. 104-113.

BRÅTHEN, K. A., FODSTAD, C. H. & GALLET, C. 2010. Ecosystem disturbance reduces the allelopathic effects of Empetrum hermaphroditum humus on tundra plants. *Journal of Vegetation Science*, 21(4), pp. 786-795.

BRÅTHEN, K. A., IMS, R. A., YOCCOZ, N. G., FAUCHALD, P., TVERAA, T. & HAUSNER, V. H. 2007. Induced shift in ecosystem productivity? Extensive scale effects of abundant large herbivores. *Ecosystems*, 10(5), pp. 773-789.

DOMAÇ, A. & SÜZEN, M. L. 2006. Integration of environmental variables with satellite images in regional scale vegetation classification. *International Journal of Remote Sensing*, 27(7), pp. 1329-1350.

ELMENDORF, S. C., HENRY, G. H., HOLLISTER, R. D., BJÖRK, R. G., BJORKMAN, A. D., CALLAGHAN, T. V., COLLIER, L. S., COOPER, E. J., CORNELISSEN, J. H. & DAY, T. A. 2012. Global assessment of experimental climate warming on tundra vegetation: heterogeneity over space and time. *Ecology Letters*, 15(2), pp. 164-175.

ENVI. 2004. ENVI User's Guide. *Research System Inc.*

FRANKLIN, S. & WULDER, M. 2002. Remote sensing methods in medium spatial resolution satellite data land cover classification of large areas. *Progress in Physical Geography*, 26(2), pp. 173-205.

GALLET, C., NILSSON, M.-C. & ZACKRISSON, O. 1999. Phenolic metabolites of ecological significance in Empetrum hermaphroditum leaves and associated humus. *Plant and Soil*, 210(1), pp. 1-9.

GOODCHILD, M. F. 1994. Integrating GIS and remote sensing for vegetation analysis and modeling: methodological issues. *Journal of Vegetation Science*, 5(5), pp. 615-626.

HALL, F. G., BOTKIN, D. B., STREBEL, D. E., WOODS, K. D. & GOETZ, S. J. 1991. Large-scale patterns of forest succession as determined by remote sensing. *Ecology*, pp. 628-640.

JOHNSTON, K., VER HOEF, J. M., KRIVORUCHKO, K. & LUCAS, N. 2001. *Using ArcGIS geostatistical analyst*. Esri Redlands.

KEECH, O., CARCAILLET, C. & NILSSON, M.-C. 2005. Adsorption of allelopathic compounds by wood-derived charcoal: the role of wood porosity. *Plant and Soil*, 272(1-2), pp. 291-300.

KERR, J. T. & OSTROVSKY, M. 2003. From space to species: ecological applications for remote sensing. *Trends in Ecology & Evolution*, 18(6), pp. 299-305.

KESHAVA, N. & MUSTARD, J. F. 2002. Spectral unmixing. *Signal Processing Magazine, IEEE*, 19(1), pp. 44-57.

LID, J. & LID, D. T. 2007. Norsk Flora. *Det Norske Samlaget, Oslo*, 7 utgåva.

MALENOVSKY, Z. 2012. Batatasin Absorption Features. *Personal communication. University of Zurich.*

MALLIK, A. U. 2008. Allelopathy: advances, challenges and opportunities. *In*: *Allelopathy in sustainable agriculture and forestry*. Springer, pp. 25-38.

MCDONALD, J. H. 2009. *Handbook of biological statistics*. Sparky House Publishing Baltimore, MD.

NILSSON, M.-C., GALLET, C. & WALLSTEDT, A. 1998. Temporal variability of phenolics and batatasin-III in Empetrum hermaphroditum leaves over an eight-year period: interpretations of ecological function. *Oikos*, pp. 6-16.

NILSSON, M.-C., ZACKRISSON, O., STERNER, O. & WALLSTEDT, A. 2000. Characterisation of the differential interference effects of two boreal dwarf shrub species. *Oecologia*, 123(1), pp. 122-128.

PELLISSIER, L., ANNE BRÅTHEN, K., POTTIER, J., RANDIN, C. F., VITTOZ, P., DUBUIS, A., YOCCOZ, N. G., ALM, T., ZIMMERMANN, N. E. & GUISAN, A.

2010. Species distribution models reveal apparent competitive and facilitative effects of a dominant species on the distribution of tundra plants. *Ecography*, 33(6), pp. 1004-1014.

R_DEVELOPMENT_CORE_TEAM. 2013. *R: A language and environment for statistical computing. R Foundation for Statistical Computing, Vienna, Austria.* Series: ISBN 3-900051-07-0, URL http://www.R-project.org/. .

REINKE, K. & JONES, S. 2006. Integrating vegetation field surveys with remotely sensed data. *Ecological Management & Restoration*, 7(s1), pp. S18-S23.

RICHARDS, J. A. & JIA, X. 1999. *Remote sensing digital image analysis*. Springer.

RUMELHART, D. E., HINTON, G. E. & WILLIAMS, R. J. 1988. *Learning representations by back-propagating errors. Chp. 8*. MIT Press, Cambridge, MA, USA.

SHEVTSOVA, A., NILSSON, M. C., GALLET, C., ZACKRISSON, O. & JÄDERLUND, A. 2005. Effects of long-term alleviation of nutrient limitation on shoot growth and foliar phenolics of Empetrum hermaphroditum. *Oikos*, 111(3), pp. 445-458.

SMITH, R. B. 2006. Introduction to hyperspectral imaging. *Microimages. Retrieved on June*, 30, p. 2008.

TYBIRK, K., NILSSON, M.-C., MICHELSEN, A., KRISTENSEN, H. L., SHEVTSOVA, A., TUNE STRANDBERG, M., JOHANSSON, M., NIELSEN, K. E., RIIS-NIELSEN, T. & STRANDBERG, B. 2000. Nordic Empetrum dominated ecosystems: function and susceptibility to environmental changes. *AMBIO: A Journal of the Human Environment*, 29(2), pp. 90-97.

U.S GEOLOGICAL SURVEY, U. 2014. Landsat Missions. *http://landsat.usgs.gov*.

VAN DER MEER, F. 1995. Spectral unmixing of landsat thematic mapper data. *International Journal of Remote Sensing*, 16(16), pp. 3189-3194.

VAN DER MEER, F. & DE JONG, S. M. 1999. Improving the results of spectral unmixing of Lansat Thematic Mapper imagery by enhancing the orthogonality of the end-members. *International Journal of Remote Sensing*, 21:15, pp. 2781-2791.

VANVOORHIS, C. R. W. & MORGAN, B. L. 2007. Understanding power and rules of thumb for determining sample sizes. *Tutorials in Quantitative Methods for Psychology*, 3(2), pp. 43-50.

WALKER, D. A., RAYNOLDS, M. K., DANIËLS, F. J., EINARSSON, E., ELVEBAKK, A., GOULD, W. A., KATENIN, A. E., KHOLOD, S. S., MARKON, C. J. & MELNIKOV, E. S. 2005. The circumpolar Arctic vegetation map. *Journal of Vegetation Science*, 16(3), pp. 267-282.

WALLSTEDT, A., GALLET, C. & NILSSON, M.-C. 2005. Behaviour and recovery of the secondary metabolite batatasin-III from boreal forest humus: influence of temperature, humus type and microbial community. *Biochemical systematics and ecology*, 33(4), pp. 385-407.

WALLSTEDT, A., NILSSON, M.-C., ODHAM, G. & ZACKRISSON, O. 1997. A method to quantify the allelopathic compound batatasin-III in extracts from Empetrum hermaphroditum using gas chromatography: applied on extracts from leaves of different ages. *Journal of chemical ecology*, 23(10), pp. 2345-2355.

WALLSTEDT, A., NILSSON, M., ZACKRISSON, O. & ODHAM, G. 2000. A link in the study of chemical interference exerted by Empetrum hermaphroditum: Quantification of batatasin-III in soil solution. *Journal of chemical ecology*, 26(6), pp. 1311-1323.

WOOKEY, P. A., AERTS, R., BARDGETT, R. D., BAPTIST, F., BRÅTHEN, K. A., CORNELISSEN, J. H., GOUGH, L., HARTLEY, I. P., HOPKINS, D. W. & LAVOREL, S. 2009. Ecosystem feedbacks and cascade processes: understanding their role in the responses of Arctic and alpine ecosystems to environmental change. *Global Change Biology*, 15(5), pp. 1153-1172.

XIE, Y., SHA, Z. & YU, M. 2008. Remote sensing imagery in vegetation mapping: a review. *Journal of Plant Ecology*, 1(1), pp. 9-23.

APPENDIX I

Table 1. "FieldSpec measurements taken in the laboratory in a previous ASD FieldSpec analyses (Ibarrola et al. unpublished data). Sample: name of the sample; Predicted value: the predicted value of Batatasin-III acquired after performing the validation with ASD FieldSpec; mg Batatasin-III: content of Batatasin-III in milligrams after being extracted from HPLC technique.

Sample	Predicted value	mg Batatasin-III
EM_BV-104-09-H_1.spc	30,77	37,98
EM_BV-104-09-H_2.spc	29,09	37,98
EM_BV-104-09-H_3.spc	33,09	37,98
EM_BV-112-09-H_1.spc	17,65	16,57
EM_BV-112-09-H_2.spc	18,96	16,57
EM_BV-112-09-H_3.spc	19,72	16,57
EM_BV-121-09-H_1.spc	23,62	21,09
EM_BV-121-09-H_2.spc	18,98	21,09
EM_BV-121-09-H_3.spc	25,33	21,09
EM_BV-122-09-H_1.spc	25,81	24,78
EM_BV-122-09-H_2.spc	31,39	24,78
EM_BV-122-09-H_3.spc	25,34	24,78
EM_BV-123-09-H_1.spc	26,47	9,98
EM_BV-123-09-H_2.spc	13,38	9,98
EM_BV-123-09-H_3.spc	22,35	9,98
EM_BV-135-10-V_1.spc	22,67	32,59
EM_BV-135-10-V_2.spc	30,08	32,59
EM_BV-135-10-V_3.spc	24,97	32,59
EM_BV-145-10-V_1.spc	30,10	19,04
EM_BV-145-10-V_2.spc	29,09	19,04
EM_BV-145-10-V_3.spc	29,70	19,04
EM_BV-146-10-V_1.spc	5,28	5,00
EM_BV-146-10-V_2.spc	15,35	5,00
EM_BV-146-10-V_3.spc	8,02	5,00
EM_BV-166-10-H_1.spc	39,21	22,32
EM_BV-166-10-H_2.spc	35,25	22,32
EM_BV-166-10-H_3.spc	35,26	22,32
EM_BV-175-10-H_1.spc	43,01	41,67
EM_BV-175-10-H_2.spc	43,78	41,67
EM_BV-175-10-H_3.spc	46,66	41,67
EM_BV-180-11-V_1.spc	23,40	27,04
EM_BV-180-11-V_2.spc	21,59	27,04
EM_BV-180-11-V_3.spc	13,18	27,04
EM_BV-181-11-V_1.spc	18,15	13,78
EM_BV-181-11-V_2.spc	15,74	13,78
EM_BV-181-11-V_3.spc	14,48	13,78
EM_BV-192-11-V_1.spc	28,50	31,14
EM_BV-192-11-V_2.spc	32,88	31,14
EM_BV-192-11-V_3.spc	25,14	31,14
EM_BV-206-11-H_1.spc	36,89	34,09
EM_BV-206-11-H_2.spc	34,27	34,09

EM_BV-206-11-H_3.spc	41,49	34,09
EM_BV-209-11-H_1.spc	47,12	45,71
EM_BV-209-11-H_2.spc	40,81	45,71
EM_BV-209-11-H_3.spc	39,31	45,71
EM_BV-211-11-H_1.spc	45,25	36,71
EM_BV-211-11-H_2.spc	45,04	36,71
EM_BV-211-11-H_3.spc	36,29	36,71
EM_BV-212-11-H_1.spc	39,76	40,95
EM_BV-212-11-H_2.spc	38,72	40,95
EM_BV-212-11-H_3.spc	41,80	40,95
EM_BV-216-11-H_1.spc	36,56	29,21
EM_BV-216-11-H_2.spc	36,37	29,21
EM_BV-216-11-H_3.spc	36,27	29,21
EM_BV-222-11-H_1.spc	21,67	23,19
EM_BV-222-11-H_2.spc	23,57	23,19
EM_BV-222-11-H_3.spc	20,22	23,19

APPENDIX II

Table 2. ASD FieldSpec data. Batatasin-III predicted value extracted from *Empetrum nigrum* leaves taken in Troms area (Tromsø, Lyfjord and Rebbenesøya). ID: name of the each sample/study place; Coverage: coverage of *Empetrum nigrum* estimated in field; Predictable ASD FieldSpec value: predicted value of Batatasin-III extracted by ASD FielSpec spectroradiometer.

ID	Coverage	Predictable ASD FieldSPec value
Tro58	10	2,17
Tro54	10	2,20
Tro55	15	2,01
Tro50	15	1,96
Tro49	15	1,95
Tro45	15	2,28
Tro52	20	2,04
Lyf13	25	1,23
Tro51	30	3,00
Tro46	30	2,06
Tro41	30	2,72
Tro37	30	1,94
Lyf12	30	0,00
Reb09	35	14,41
Reb07	40	31,82
Lyf26	40	26,01
Lyf16	40	7,31
Tro47	50	2,64
Reb08	50	29,07
Lyf20	50	35,41
Lyf25	55	13,07
Tro42	60	1,79
Lyf21	60	28,89
Lyf17	60	11,36
Tro40	70	1,55
Tro36	70	2,09
Lyf18	70	13,25
Lyf14	70	16,49
Lyf11	70	0,00
Reb06	80	23,52
Lyf30	80	10,51
Lyf29	80	10,68
Lyf23	80	9,04
Lyf24	84	4,64
Lyf27	85	4,29
Lyf19	85	0,73

Tro44	90	1,48
Tro39	90	1,98
Tro34	90	2,36
Lyf10	90	8,94
Tro38	95	2,51
Tro33	95	1,32
Tro31	95	2,48
Reb05	95	9,58
Reb04	95	28,57
Tro35	97	1,56
Tro32	97	2,03
Reb03	100	18,09
Reb02	100	30,98
Reb01	100	17,04

APPENDIX III

Table 3. Data recorded during field work in Tromsø and Ifjord study areas. ID: name of the sample/study point; Area: area where the study point was sampled; County: name of the area where the study point was placed, either Troms of Ifjord; zone: UTM zone of the coordinates; x: x UTM coordinate of the study point; y: y UTM coordinate of the study point. Coverage (%): coverage of *Empetrum nigrum* estimated in field.

ID	AREA	COUNTY	zone	x	y	Coverage (%)
1209_01	Kvaloya-Tromso	Troms	34W	416885	7734157	85
1209_02	Kvaloya-Lyfjord 1	Troms	34W	417041	7740334	85
1209_03	Kvaloya-Lyfjord 2	Troms	34W	417158	7740388	35
1209_04	Kvaloya-Risvik	Troms	34W	419341	7748562	80
1209_05	Kvaloyvagen 1	Troms	34W	416712	7750051	87
1209_06	Kvaloyvagen 2	Troms	34W	415153	7749257	30
1209_07	Kvaloya-South Tromso/Hakoya	Troms	34W	414188	7725754	50
1209_08	Kvaloya-South Tromso/Hakoya (Dogs' Center)	Troms	34W	414216	7725626	65
1209_09	Kvaloya (Area 2) 1 - Up hill	Troms	34W	401303	7728953	75
1209_10	Kvaloya (Area 2) 2 - Down hill	Troms	34W	401766	7728953	80
1209_11	Kvaloya-Sommaroy	Troms	34W	384517	7721348	65
1209_12	Road 91/Station 1 - Middle hill	Troms	34W	431471	7718635	53,75
1209_13	Road 91/Station 2 - Up hill	Troms	34W	431486	7718479	66,25
1209_14	Lyngen-Svensy 1	Troms	34W	456781	7723078	77,5
1209_15	Lyngen-Svensy 2	Troms	34W	456635	7723454	80,83
1209_16	Skibotn 1	Troms	34W	482698	7680922	63,3
1209_17	Skibotn 2	Troms	34W	482701	7680736	48,33
1209_18	Kilpis 1	Troms	34W	488362	7674153	80,41
1209_19	Kilpis 2	Troms	34W	488115	7674190	42,08

1209_20	Skogsfjord 1	Troms	34W	433218	7761203	85,41
1209_21	Skogsfjord 2	Troms	34W	433228	7761334	82,5
1209_22	Skogsfjord 3	Troms	34W	433282	7761495	83,3
1306_23	Ifjord 1_23	Ifjord	35W	513085	7814048	85,42
1306_24	Ifjord 2_24	Ifjord	35W	513241	7814452	85,83
1306_25	Ifjord 3_25	Ifjord	35W	513138	7814261	70,83
1306_26	Ifjord 4_26	Ifjord	35W	512980	7813828	89,58
1306_27	Ifjord 5_27	Ifjord	35W	513399	7813889	92,08
1306_28	Ifjord 6_28	Ifjord	35W	511321	7814956	81,67
1306_29	Ifjord 7_29	Ifjord	35W	511556	7814390	77,08
1306_30	Ifjord 8_30	Ifjord	35W	511462	7814257	93,75
1306_31	Ifjord 9_31	Ifjord	35W	511437	7814184	15,42
1306_32	Ifjord 10_32	Ifjord	35W	511881	7815068	79,58
1306_33	Ifjord 11_33	Ifjord	35W	511842	7815490	90,00
1306_34	Ifjord 12_34	Ifjord	35W	513352	7815076	97,50
1306_35	Ifjord 13_35	Ifjord	35W	513468	7815506	94,58
1306_36	Ifjord 14_36	Ifjord	35W	518202	7814353	82,50
1306_37	Ifjord 15_37	Ifjord	35W	517916	7814075	90,42
1306_38	Ifjord 16_38	Ifjord	35W	518078	7813959	94,58
1306_39	Ifjord 17_39	Ifjord	35W	519841	7813168	78,75
1306_40	Ifjord 18_40	Ifjord	35W	511063	7814016	79,17
1306_41	Ifjord 19_41	Ifjord	35W	510802	7813900	92,92
1306_42	Ifjord 20_42	Ifjord	35W	510926	7813885	73,75
1306_43	Ifjord 21_43	Ifjord	35W	511198	7814115	97,50
1306_44	Ifjord22_44	Ifjord	35W	513040	7815495	92,08
1306_45	Ifjord23_45	Ifjord	35W	513319	7815744	74,17
1306_46	Ifjord24_46	Ifjord	35W	513281	7815008	98,33

1306_47	Ifjord25_47	Ifjord	35W	513154	7814860	90,83
1306_48	Rebbenes	Troms	34W	414585	7770360	94,17
1306_49	Hansnes_1	Troms	34W	446502	7768905	96,25
1306_50	Hansnes_2	Troms	34W	446635	7768669	85,00

APPENDIX IV

Table 4. Extracted values of *Empetrum nigrum* from the spectral unmixing classification performed in ENVI. ID: name of the sample/study point; Area: area where the study point was sampled; SUM Extraction: Spectral Unmixing extracted values of *Empetrum nigrum*; SUM % Extraction: Spectral Unmixing extracted values of *Empetrum nigrum* in percentage; % Field Coverage: coverage of *Empetrum nigrum* estimated in field.

ID	AREA	SUM Extraction	SUM % Extraction	% Field Coverage
1209_01	Kvaloya-Tromso	229	89,453125	85
1209_04	Kvaloya-Risvik	195	76,171875	80
1209_06	Kvaloyvagen 2	148	57,8125	30
1209_07	Kvaloya-South Tromso/Hakoya	107	41,796875	50
1209_08	Kvaloya-South Tromso/Hakoya (Dogs' Center)	181	70,703125	65
1209_09	Kvaloya (Area 2) 1 - Up hill	127	49,609375	75
1209_10	Kvaloya (Area 2) 2 - Down hill	188	73,4375	80
1209_11	Kvaloya-Sommaroy	202	78,90625	65
1209_14	Lyngen-Svensy 1	154	60,15625	77,5
1209_15	Lyngen-Svensy 2	235	91,796875	80,83
1209_16	Skibotn 1	255	99,609375	63,3
1209_18	Kilpis 1	255	99,609375	80,41
1209_19	Kilpis 2	134	52,34375	42,08
1209_20	Skogsfjord 1	255	99,609375	85,41
1209_21	Skogsfjord 2	181	70,703125	82,5
1209_22	Skogsfjord 3	249	97,265625	83,3
1306_23	Ifjord 1_23	113	44,140625	85,42
1306_24	Ifjord 2_24	107	41,796875	85,83
1306_25	Ifjord 3_25	57	22,265625	70,83

1306_26	Ifjord 4_26	112	43,75	89,58
1306_27	Ifjord 5_27	137	53,515625	92,08
1306_28	Ifjord 6_28	126	49,21875	81,67
1306_29	Ifjord 7_29	124	48,4375	77,08
1306_30	Ifjord 8_30	140	54,6875	93,75
1306_32	Ifjord 10_32	86	33,59375	79,58
1306_33	Ifjord 11_33	134	52,34375	90,00
1306_34	Ifjord 12_34	136	53,125	97,50
1306_35	Ifjord 13_35	199	77,734375	94,58
1306_36	Ifjord 14_36	174	67,96875	82,50
1306_37	Ifjord 15_37	176	68,75	90,42
1306_38	Ifjord 16_38	214	83,59375	94,58
1306_39	Ifjord 17_39	179	69,921875	78,75
1306_40	Ifjord 18_40	69	26,953125	79,17
1306_41	Ifjord 19_41	173	67,578125	92,92
1306_42	Ifjord 20_42	78	30,46875	73,75
1306_43	Ifjord 21_43	126	49,21875	97,50
1306_44	Ifjord22_44	179	69,921875	92,08
1306_45	Ifjord23_45	151	58,984375	74,17
1306_46	Ifjord24_46	167	65,234375	98,33
1306_47	Ifjord25_47	167	65,234375	90,83
1306_48	Rebbenes	242	94,53125	94,17
1306_49	Hansnes_1	181	70,703125	96,25
1306_50	Hansnes_2	195	76,171875	85,00

APPENDIX V

Table 5. Residual Error data. ID: name of the sample/study point; Area: area where the study point was sampled; Total Residual Error: residual error in both areas combined; Ifjord Residual Error: residual error in Ifjord area. Tromsø Residual Error: residual error in Tromsø area.

ID	AREA	Total Residual Error	Ifjord Residual Error	Tromsø Residual Error
1209_01	Kvaloya-Tromso	24,33		6,58
1209_04	Kvaloya-Risvik	11,91		-3,80
1209_06	Kvaloyvagen 2	2,17		6,83
1209_07	Kvaloya-South Tromso/Hakoya	-17,29		-20,78
1209_08	Kvaloya-South Tromso/Hakoya (Dogs' Center)	9,03		-0,57
1209_09	Kvaloya (Area 2) 1 - Up hill	-13,79		-27,46
1209_10	Kvaloya (Area 2) 2 - Down hill	9,17		-6,54
1209_11	Kvaloya-Sommaroy	17,23		7,63
1209_14	Lyngen-Svensy 1	-3,68		-18,37
1209_15	Lyngen-Svensy 2	27,39		11,34
1209_16	Skibotn 1	38,23		29,32
1209_18	Kilpis 1	35,27		19,40
1209_19	Kilpis 2	-5,38		-5,64
1209_20	Skogsfjord 1	34,41		16,50
1209_21	Skogsfjord 2	6,01		-10,72
1209_22	Skogsfjord 3	32,43		15,38
1306_23	Ifjord 1_23	-21,06	-8,45	
1306_24	Ifjord 2_24	-23,47	-11,24	
1306_25	Ifjord 3_25	-40,42	-14,21	
1306_26	Ifjord 4_26	-22,17	-13,43	

1306_27	Ifjord 5_27	-12,83	-6,43	
1306_28	Ifjord 6_28	-15,33	0,77	
1306_29	Ifjord 7_29	-15,32	5,06	
1306_30	Ifjord 8_30	-11,95	-7,10	
1306_32	Ifjord 10_32	-30,60	-12,54	
1306_33	Ifjord 11_33	-13,65	-5,30	
1306_34	Ifjord 12_34	-14,16	-12,81	
1306_35	Ifjord 13_35	10,96	15,03	
1306_36	Ifjord 14_36	3,27	18,61	
1306_37	Ifjord 15_37	2,69	10,64	
1306_38	Ifjord 16_38	16,81	20,89	
1306_39	Ifjord 17_39	5,87	24,70	
1306_40	Ifjord 18_40	-37,17	-18,73	
1306_41	Ifjord 19_41	1,09	6,71	
1306_42	Ifjord 20_42	-32,72	-9,23	
1306_43	Ifjord 21_43	-18,06	-16,71	
1306_44	Ifjord22_44	3,57	9,98	
1306_45	Ifjord23_45	-4,27	18,82	
1306_46	Ifjord24_46	-2,19	-1,61	
1306_47	Ifjord25_47	-0,90	6,67	
1306_48	Rebbenes	27,82		6,34
1306_49	Hansnes_1	3,64		-18,69
1306_50	Hansnes_2	11,05		-6,70